

# The Portuguese Large Wildfire Spread Database (PT-FireSprd)

Akli Benali<sup>1</sup>, Nuno Guiomar<sup>2</sup>, Hugo Gonçalves<sup>3,4</sup>, Bernardo Mota<sup>5</sup>, Fábio Silva<sup>3,4</sup>, Paulo M. Fernandes<sup>6</sup>, Carlos Mota<sup>3,4</sup>, Alexandre Penha<sup>4</sup>, João Santos<sup>3,4</sup>, José M.C. Pereira<sup>1,7</sup>, Ana C.L. Sá<sup>1</sup>

<sup>1</sup>Centro de Estudos Florestais, Instituto Superior de Agronomia, Universidade de Lisboa, Tapada da Ajuda, 1349-017 Lisboa, Portugal

<sup>2</sup>MED - Mediterranean Institute for Agriculture, Environment and Development; CHANGE - Global Change and Sustainability; EaRSLab - Earth Remote Sensing Laboratory Institute; IIFA - Institute for Advanced Studies and Research; University of Évora, 7006-554 Évora, Portugal

<sup>3</sup>Força Especial de Proteção Civil, 2080-221 Almeirim, Portugal

<sup>4</sup>Autoridade Nacional de Emergência e Proteção Civil, 2799-51 Carnaxide, Portugal

<sup>5</sup>National Physical Laboratory (NPL), Climate Earth Observation (CEO), Hampton Rd. Teddington, TW11 0LW, UK

<sup>6</sup>CITAB - Centro de Investigação e de Tecnologias Agro-Ambientais e Biológicas, Universidade de Trás-os-Montes e Alto Douro, 5001-801 Vila Real, Portugal;

<sup>7</sup>Laboratório Associado TERRA, Tapada da Ajuda, 1349-017 Lisboa, Portugal

*Correspondence to:* Akli Benali (aklibenali@gmail.com)

**Abstract.** Wildfire behaviour depends on complex interactions between fuels, topography and weather, over a wide range of scales, being important for fire research and management applications. To allow for a significant progress towards better fire management, the operational and research communities require detailed open data on observed wildfire behaviour. Here, we present the Portuguese Large Wildfire Spread Database (PT-FireSprd) that includes the reconstruction of the spread of 80 large wildfires that occurred in Portugal between 2015 and 2021. It includes a detailed set of fire behaviour descriptors, such as rate-of-spread (ROS), fire growth rate (FGR), and fire radiative energy (FRE). The wildfires were reconstructed by converging evidence from complementary data sources, such as satellite imagery/products, airborne and ground data collected by fire personnel, official fire data and information in external reports. We then implemented a digraph-based algorithm to estimate the fire behaviour descriptors and combined it with MSG-SEVIRI fire radiative power estimates. A total of 1197 ~~observations of ROS and FGR were estimates were calculated estimated~~ along with 609 FRE estimates. The extreme fires of 2017 were responsible for the maximum observed values of ROS (~~8956-8900~~ m/h) and FGR (~~4436-4400~~ ha/h). Combining both descriptors, we ~~defined-describe the 6~~ fire behaviour ~~distribution using six percentile intervals classes~~ that can be easily communicated to both research and management communities ~~and support a wide number of applications~~. Analysis ~~of the database also~~ showed that ~~the area~~ burned by ~~a extent wildfire~~ is mostly determined by ~~its~~-FGR rather than by ~~its forward speed~~ROS. Finally, we explored a practical example to show how the PT-FireSprd database can be used to study the dynamics of individual wildfires and to build robust case studies for training and capacity building.

The PT-FireSprd is the first open access fire progression and behaviour database in Mediterranean Europe, dramatically expanding the extant information. Updating the PT-FireSprd database will require a continuous joint effort by researchers and

35 fire personnel. PT-FireSprd data are publicly available through <https://doi.org/10.5281/zenodo.7495506> (last access: 30th  
36 December 2022) and have a large potential to improve current knowledge on wildfire behaviour and support better decision-  
37 making (Benali et al. 2022).

38

39 **Keywords:** fire behaviour; satellite; airborne; ground data; rate of spread; fire radiative energy; graphs; progression

40

## 41 1 Introduction

42 Wildfire behaviour is broadly defined as the way a free-burning fire ignites, develops and spreads through the landscape (Albini  
43 1984; Rothermel 1972). It depends on complex interactions between fuels, topography and weather, over a wide range of  
44 temporal and spatial scales (Santoni et al., 2011; Countryman, 1972). Wildfire behaviour can be described using common  
45 metrics such as the spread rate, ~~propagation mode~~, area-growth rate, ~~perimeter~~, rate of energy release and flame ~~size-length~~  
46 (Albini 1984). Fire behaviour ~~data information~~ is important for fire research and management applications (Finney et al.,  
47 2021).

48  
49 To allow for a significant progress towards better fire management, the operational and research communities require detailed  
50 open data on observed wildfire behaviour (Gollner et al., 2015). In this context, systematic mapping of the fire front progression  
51 through space and time is critical to address existing needs, ~~particularly for of~~ wildfires burning under a wide range of  
52 environmental conditions, ~~including extreme ones~~ (Storey et al., 2021; Gollner et al., 2015). Compiling quality fire behaviour  
53 information is ~~paramount important~~ to develop reliable and well-suited fire spread models and for a much-needed extensive  
54 evaluation of fire behaviour predictions, which is ~~crucial paramount for its ultimate aim to~~ support the decision-making process  
55 (Alexander and Cruz, 2013a; Scott and Reinhardt, 2001). This includes planning pre-suppression activities and defining  
56 resources dispatch to wildfires, delineating safe and effective fire suppression strategies and tactics during a wildfire, and for  
57 early alert and evacuation purposes (Finney et al., 2021). Comprehensive fire progression and behaviour information is also  
58 useful to develop burned area/fire perimeter mapping algorithms (Valero et al., 2018), understand fire effects (Collins et al.,  
59 2009), fire danger rating (Parisien et al., 2011), fire hazard mapping and risk analysis (Alcasena et al., 2021, Palaiologou et  
60 al., 2020), planning and implementation of preventive fuel treatments (Salis et al., 2018), and also to foster robust training of  
61 operative personnel and researchers improving their learnings from past wildfires (Alexander and Thomas, 2003).  
62 Unfortunately, reliable quality information on the progression and behaviour of wildfires, especially those burning under  
63 extreme conditions, is difficult to collect (Gollner et al., 2015).

64  
65 Fire behaviour data can be collected from laboratory experiments, experimental fires, prescribed fires or wildfires. A large  
66 number of laboratory-scale experiments have been made for the development of semi-empirical rate-of-spread (ROS) models  
67 (Rothermel 1972; Catchpole et al., 1998). Experimental fires have been set up to collect fireline data, estimate fire behaviour  
68 descriptors and develop empirical fire spread models (Forestry Canada Fire Danger Group 1992; Fernandes et al., 2009; Cruz  
69 et al., 2015; ~~Gollner et al., 2015~~), requiring significant time and resources. Neither laboratory-scale nor experimental fires  
70 represent the spatial and temporal variability of environmental conditions under which uncontrolled wildfires most often burn  
71 (e.g. Gollner et al., 2015).

72

73 Due to the unpredictability of their timing and location, conventional measurements on wildfires are difficult to perform and  
74 lead to slow accumulation of data (Alexander & Cruz 2013b). Generally, they are of poor quality or incomplete (Duff et al.,  
75 2013), although outstanding reconstruction examples exist (e.g. Wade & Ward 1973; Alexander & Lanoville 1987; Cheney  
76 2010). Dedicated efforts do exist (Vaillant et al., 2014), but wildfire behaviour estimates often result from opportunistic  
77 observations (e.g. Santoni et al., 2011) or post-fire interviews (e.g. Butler and Reynolds, 1997). Some authors have made  
78 relevant efforts in compiling a large amount of ~~direct~~ field observations on wildfire behaviour (Alexander and Cruz, 2006;  
79 Cheney et al., 2012), some combined with experimental fire data (Cruz and Alexander, 2013, 2019; Anderson et al., 2015;  
80 Cruz et al., 2018, 2021, 2022; Khanmohammadi et al., 2022). An additional limitation lies on the fact that some of the existing  
81 fire behaviour datasets are not freely available ~~for to~~ the operational and research communities (Gollner et al., 2015).

82  
83 Remote sensing technology, either through airborne or satellite platforms, can provide relevant data to document wildfires  
84 propagation. Manned or unmanned airborne visible and infrared (IR) images have been ~~collected-used~~ to document-map fire  
85 progression, ~~and in some cases to retrieve fire radiative power estimates~~ (Schag et al., 2021; Storey et al., 2020, 2021; Coen  
86 & Riggan 2014; Sharples et al., 2012). Satellite data provide easy-to-use, autonomous, synoptic observations of fire activity  
87 ~~throughout the entire globe worldwide~~. Recent advances in satellite technology have made available a panoply of open-access  
88 imagery and products with capabilities to monitor wildfires over the entire globe. Their characteristics vary in resolution,  
89 ranging from high (10-30 m) to low (4-5 km), and frequency of overpass, ranging from 5-15 days to every 15 minutes. To  
90 monitor wildfire progression, satellites provide imagery and products that identify where a fire is actively burning at the time  
91 of overpass (“thermal anomalies” or “active fire” products). ~~that range from moderate to high spatial resolution, and from~~  
92 ~~every 5 days to sub-daily frequency~~. Several authors have used satellite data to map daily fire progression at the country-level  
93 (Parks et al., 2014; Veraverbeke et al., 2014, Briones-Herrera et al., 2020; Sá et al., 2017) and at the global scale (Artés et al.,  
94 2019; Oom et al., 2016). Some have estimated fire behaviour metrics, such as ROS (Humber et al., 2022; Frantz et al., 2017;  
95 Andela et al., 2019). Recently, Chen et al., (2022) improved this ~~line of~~ research line by using Visible Infrared Imaging  
96 Radiometer Suite (VIIRS) data to automatically reconstruct sub-daily fire progression at a higher resolution. Other authors  
97 exploited the capabilities of geostationary satellites to monitor wildfires and estimate fire behaviour descriptors (Sifakis et al.,  
98 2011; Storey et al., 2021).

99  
100 The different data sources used to characterise wildfire progression and behaviour have inherent limitations and potentialities.  
101 Ground-collected data can be characterised by large uncertainties, particularly when taken by fire personnel whose focus is on  
102 suppression and not on data collection (Alexander and Thomas, 2003). In addition, ground-collected data have poor synoptic  
103 capability and provide a limited representation of fire behaviour variability. For example, ~~distribution, distribution~~ of ROS  
104 values for single fire runs are seldom available (Cruz, 2010). Airborne data can provide wider coverage of the fire progression,  
105 ~~however although~~, have limited temporal acquisition windows (e.g. USFS National Infrared Operations - NIROPS - provides

106 data once per night) and in some cases require manual digitization of fire perimeters (Stow et al. 2014; Veraverbeke et al.,  
107 2014; Storey et al. 2021).

108  
109 The tradeoff between spatial and temporal resolution of satellite data, as well as the presence of clouds and thick smoke can  
110 significantly limit their fire monitoring capability. In addition, the correct location of a wildfire cannot be determined inside a  
111 burning pixel whose size varies with viewing geometry and sensor properties (Wolfe et al., 1998). Daily or sub-daily satellite-  
112 derived fire progressions can also fail to reflect the influence of extreme conditions in fire behaviour due to the effect of  
113 averaging over relatively long periods (Collins et al., 2009).

114  
115 Considering that all data sources have limitations and provide information for very limited ~~time frames~~ periods, combining  
116 different sources is key to capture the spread and behaviour variability of wildfires. The example provided in Figure 1  
117 highlights the potential of combining different data sources to overcome inherent acquisition gaps, particularly in the afternoon,  
118 when both field and airborne data overcome the satellite gap, and during dawn, when ground-collected and satellite data  
119 complement each other. Note that observation frequencies of ground and airborne data strongly depend on daily fire activity  
120 patterns.

121  
122 **(Figure 1 near here)**

123  
124 Systematic multi-source acquisition of wildfire data collection was recently done by Kilinc et al., (2012) and Storey et al.,  
125 (2020, 2021) for Australia, by Crowley et al., (2019) for Canada (only satellite data) and by Fernandes et al., (2020) at the  
126 global scale. The pursuit of this goal requires a monitoring framework and a concerted joint effort between research and  
127 operational communities (Stocks et al., 2004; McCaw et al., 2012, Storey et al., 2020, 2021). Additional data on constantly  
128 evolving wildfires, accompanied by robust replicable methods, is needed, namely in southern Europe where there is a  
129 substantial data gap ~~is manifest~~ (Fernandes et al., 2018).

130  
131 Here, we present the Portuguese Large Wildfire Spread Database (PT-FireSprd), ~~which that~~ combines data from multiple  
132 sources, using a “convergence of evidence” approach to characterise in detail the progression and behaviour of large wildfires  
133 in Portugal. Fire behaviour is described *in-sensu stricto*, thus analysis of its drivers, namely weather and fuel, -and effects is  
134 beyond the scope of the current work. The work results from a joint co-creation effort between researchers and fire personnel,  
135 integrating data collected from airborne and ground operational resources.

## 136 2 Data and Methods

### 137 2.1 Overview

138 We first collected data for all the large wildfires (>100 ha) that occurred in mainland Portugal –between 2015 and 2021. Out  
139 of 14,973 wildfires that occurred during this period, 793 (about 5%) had an extent larger than 100 ha. These ~~large wildfires~~  
140 were responsible for almost 1 million hectares burned ~~during this period~~, of which half occurred in the extreme fire season of  
141 2017. About 90% of the total burned area resulted from the 760 ~~larger-largest~~ wildfires.

142 Multi-source input data (L0, section 2.2) were collected and only wildfires with good quality data and representative ~~data of~~  
143 its spread were kept. Fire progressions were reconstructed from the input data and fire behaviour metrics were estimated. The  
144 PT-FireSprd database was then organised in three levels:

- 145 • L1: Wildfire ~~Progression-progression~~ (section 2.3), representing the spatial and temporal evolution of the wildfire  
146 spread (i.e. where and when).
- 147 • L2: Wildfire behaviour (section 2.4), including quantitative behaviour descriptors of how a wildfire burned, such as  
148 the rate-of-spread (ROS), fire growth rate (FGR), fire radiative energy (FRE), and FRE flux;
- 149 • L3: Simplified ~~Wildfire-wildfire~~ behaviour (section 2.5), averaging ~~fire~~ behaviour descriptors over longer periods  
150 that represent relatively homogenous fire runs.

151 The data from the different levels ~~is-were~~ composed by a large set of maps that can be useful for several applications and target  
152 users. For example, L1 data can be used by fire analysts or researchers to evaluate suppression strategies and understand the  
153 fire spread drivers or to evaluate burned area/fire perimeter mapping algorithms. L2 data ~~is-are~~ useful, for example, to calibrate  
154 existing or build better fire spread models, while potential applications of L3 are improving fire danger rating, fire hazard  
155 mapping and risk analysis. The overall flow of the data and methods is described in Figure 2.

156  
157 **(Figure 2 near here)**

158

### 159 2.2 Input Data (L0)

160 To reconstruct the wildfire progressions, we used data acquired by satellites, from airborne sources and in the field by fire  
161 personnel. Most of ~~this-these~~ data ~~is-are~~ currently integrated in a near-real time operational WEB-GIS fire monitoring platform  
162 (in Portuguese “FEB Monitorização”, hereafter FEBMON) developed in 2018 by the Civil Protection Special Force (FEPC)  
163 and the Portuguese National Authority for Emergency and Civil Protection (ANEPC). The data were complemented with  
164 official fire data (~~e.g., ignition date and location~~) and information from external reports. Table A1 summarizes the different  
165 data sources used and their main characteristics.

166

## 167 2.2.1 Satellite data

168 ~~Satellite data was used to support the reconstruction of past wildfire spread. Currently, there are many sources of open access~~  
169 ~~satellite data with capabilities to monitor wildfires over the entire globe. Their characteristics vary in resolution, ranging from~~  
170 ~~high (10-30 m) to low (4-5 km), and frequency of overpass, ranging from 5-15 days to every 15 minutes. To monitor wildfire~~  
171 ~~progression, satellites provide imagery and products that identify the location where a fire is actively burning at the time of~~  
172 ~~overpass (“thermal anomalies” or “active fire” products).~~

173  
174 The Sentinel-2 Multispectral Instrument (MSI) and the Landsat 8/9 Operational Land Imager (OLI) provide images ~~of the~~  
175 ~~Earth’s surface~~ on average every 5 days ~~and every 16 days, respectively when combined. Their, with a~~ spatial resolution ~~ranges~~  
176 ~~ranging~~ between 10 and 60 m ~~depending on the spectral band~~. PROBA-V has a ~~lower~~ number of spectral bands (4) ~~when~~  
177 ~~compared with other satellites used~~ and provides daily images at 300 m of spatial resolution, and every 5 days with a 100 m  
178 spatial resolution. The VIIRS instrument aboard the NPP and NOAA-20 satellites, collects data on average twice per day with  
179 a resolution ~~varying of between~~ 375 m ~~to and~~ 750 m, ~~depending on the spectral band~~. The Moderate-Resolution Imaging  
180 Spectroradiometer (MODIS) is an instrument on board the TERRA and AQUA satellites with spatial resolutions ranging from  
181 250 m to 1000 m, ~~depending on the spectral bands,~~ providing on average four daily revisits when combined. Sentinel-3  
182 satellites have onboard the Sea and Land Surface Temperature Radiometer (SLSTR) and the Ocean and Land Color Instrument  
183 (OLCI), with spatial resolutions ranging between 500 and 1000 m for the former, and 300 m for the latter. Data ~~is are~~ acquired  
184 ~~on average~~ twice per day ~~on average~~, but the OLCI does not retrieve ~~night time~~ nighttime data.

185  
186 We used ~~L2-atmospherically corrected (L2)~~ satellite imagery ~~from the above mentioned sensors~~ to create false colour  
187 composites that could highlight burned areas (low NIR, high SWIR reflectance), active flaming areas (high SWIR and/or TIR  
188 reflectance) and unburned vegetation (high NIR reflectance). ~~The bands used in the false colour composites depend on spectral~~  
189 ~~characteristics of each sensor.~~ Typical false colour composites ~~contain use~~ bands 12-8A-4 of Sentinel-2, bands 7-2-1 for  
190 MODIS and bands 1-2-4 for PROBA-V. Most imagery were downloaded from Sentinel EO Browser ([https://apps.sentinel-](https://apps.sentinel-hub.com/eo-browser/)  
191 [hub.com/eo-browser/](https://apps.sentinel-hub.com/eo-browser/)), Worldview (<https://worldview.earthdata.nasa.gov/>) and VITO-EODATA ([https://www.vito-](https://www.vito-eodata.be/PDF/)  
192 [eodata.be/PDF/](https://www.vito-eodata.be/PDF/)) which allow easy and fast access to historical L2 data.

193  
194 To complement the satellite imagery, we used the thermal anomaly products of VIIRS (VNP14IMGML-C1, Schroeder et al.,  
195 2014, 2017) and MODIS (MCD14ML-C6, Giglio et al., 2003, 2016), with 375 m and 1 km resolution at nadir, respectively.  
196 Data ~~is are~~ available at [fuoco.geog.umd.edu](http://fuoco.geog.umd.edu) and FIRMS (<https://firms.modaps.eosdis.nasa.gov/>). These products allow  
197 estimating the approximate location and timing of an active wildfire, and ~~also~~ provide an estimate of the fire radiative power  
198 (FRP), a proxy of the radiant energy released per time unit, and ~~a~~ proxy for fuel consumption and fireline intensity. In addition,  
199 coarse resolution data (~4 km) from the Spinning Enhanced Visible and Infrared Imager (SEVIRI) sensor onboard the Meteosat

200 Second Generation (MSG) geostationary satellite, was used to characterise the temporal evolution of fire activity using FRP  
201 estimates every 15 min<sup>2</sup> (Wooster et al., 2015). Data ~~is~~are available at [https://landsaf.ipma.pt/en/products/fire-](https://landsaf.ipma.pt/en/products/fire-products/frpgrid/)  
202 [products/frpgrid/](https://landsaf.ipma.pt/en/products/fire-products/frpgrid/). The FRP detections associated with each wildfire were identified using a spatial-temporal nearest distance  
203 algorithm. An empirical threshold derived from the analysis of a selected number of wildfires was used to account for the  
204 satellite pixel geolocation and temporal reporting uncertainties. ~~For each wildfire, the~~ Fire Radiative Energy (FRE), ~~and~~  
205 ~~associated uncertainties, were~~was estimated based on the FRP detections, by assuming a constant rate of energy release every  
206 15 min, integrating FRP detections over 30' periods and by assuming a constant rate of energy release and then aggregated in  
207 30 min bins (Eq. 1):

$$208 \text{FRE}_i = 0.0009 \times (\sum_{k=1}^2 \text{FRP}_k), \quad (1)$$

209 where index i indicates ~~the a~~ 30 min<sup>2</sup> bin, index k indicates the ~~15' 15 min~~ FRP value in MW, and the 0.0009 factor converts  
210 the sum into TJ (Pinto et al. 2017).

### 211 2.2.2 Airborne data

212 Some aeroplanes and helicopters that operate during wildfires collect photos and videos. Data are collected during the initial  
213 attack (i.e. up to 90 min after the alert) by the heli-brigades of the National Guard (GNR) using their mobile phones, and  
214 occasionally, during extended attack. Aeroplanes, operated by FEPC\ANEPC since 2018 (AVRAC), ~~are equipped with a~~  
215 ~~gimbal that contains~~carry visible and thermal cameras ~~that,~~collecting photos and videos during extended attack covering the  
216 entire active fire perimeter. In addition, helicopters that coordinate aerial ~~suppression,~~suppression also collect ~~valuable~~  
217 ~~information regarding fire progression~~photos and videos. Both data sources collect data only during daytime (~~with a very~~  
218 ~~small number few~~of exceptions), at relatively low altitudes.

219  
220 ~~These a~~ Airborne data are systematically uploaded in real-time in FEBMON ~~since 2018~~, providing high quality information  
221 regarding the probable location of the fire start, active flaming zones, and specially wildfire progression. It is noteworthy to  
222 mention that airborne footage is not synoptic, as different parts of the wildfire (e.g. left flank vs. right flank) are captured at  
223 different moments, ~~which,~~ ~~These,~~ depending on the fire extent and operational priorities, can result in ~~be characterised by~~  
224 ~~significant~~large acquisition time lags.

### 225 2.2.3 Ground data

226 The FEBMON system is linked to ~~user friendly~~ portable ~~tools devices~~ that allow collecting ~~of~~ georeferenced ground data  
227 during wildfires. ~~These tools are typically installed in mobile phones and tablets and are used~~ by fire personnel from several  
228 ~~organisations entities~~ (e.g., fire fighters, forest service). Ground-collected data consists of three main types: i) photos and  
229 videos; ii) points that identify active flaming combustion, inactive flaming or smouldering or locations requiring mop-up  
230 ~~activities~~; iii) polygons that delineate an area burned until the time of acquisition (i.e. fire progression).

231

232 Besides the data automatically linked to FEBMON, valuable ad-hoc information ~~can be was~~ used to reconstruct wildfire spread,  
233 such as additional photos ~~and~~ videos ~~captured on the ground~~, and post-fire interviews. In sum, data collected by fire personnel  
234 in the field provided valuable spatiotemporal information regarding wildfire spread, ignition and/or wildfire re-activation.

#### 235 **2.2.4 Official fire data**

236 ~~The Forest Service (in Portuguese, “Instituto da Conservação Natureza e das Florestas” – ICNF) provides a fire database with~~  
237 ~~the~~ ~~The final~~ burned area perimeters for the entire country ~~were provided by ICNF (-Instituto da Conservação da Natureza e~~  
238 ~~das Florestas).~~ derived from a combination of fieldwork and satellite data (<https://geocatalogo.icnf.pt/>). ~~We found some e~~Errors  
239 in the ~~final burned area~~ perimeters ~~that~~ were corrected manually ~~with using~~ Sentinel-2 or Landsat 8/9 post-fire false colour  
240 composites (see section 2.2.1). ~~For a very limited number of very large multi-day wildfires, In addition, for a very limited~~  
241 ~~number of very large multi day wildfires,~~ we used burned ~~area perimeters~~ areas (resolution of 1.5 m) provided by the  
242 Copernicus Emergency Management Service (<https://emergency.copernicus.eu/mapping/>);-

243  
244 ~~Regarding ignition data, we used the~~ ~~The Forest Service also provides information regarding th~~ ~~official~~ wildfire ~~wildfire~~ start  
245 location, ~~typically derived from post-fire investigation (ICNF, mostly based on post fire investigation done by GNR personnel~~  
246 ~~(SGIF, <https://fogos.icnf.pt/sgif2010/>), the ignition location provided by first responders and time of alert (ANEPC).~~ Ignition  
247 data have several known issues (Pereira et al., 2011) the most relevant of which, for the purposes of the present study, is the  
248 accuracy of its exact location.

249  
250 ~~Finally, we analysed the official wildfire time logs from ANEPC, which seldom contain useful contextual information on~~  
251 ~~wildfire location at a given date/hour.~~

252  
253  
254 ~~ANEPC manages the Operation Decision Support System (SADO) that includes information, such as i) date/hour of the~~  
255 ~~wildfire alert; ii) ignition location provided by first responders; and iii) a time log that seldom contains useful contextual~~  
256 ~~information on wildfire location at a given date/hour.~~

#### 257 **2.2.4-5 Reports of 2017 large wildfires**

258 We ~~also~~ used ignition and fire progression data published in reports ~~on the dynamics~~ of the very large wildfires of June 2017,  
259 including the Pedrogão Grande wildfire, and ~~of~~ October 2017 (Guerreiro et al., 2017, 2018; Viegas et al., 2019). Regarding  
260 Guerreiro et al. (2017, 2018), the primary data sources used to reconstruct the fire progression were satellite imagery, ~~thermal~~  
261 ~~anomaly active fire~~ data and burned area perimeters provided by the Copernicus Emergency Management Service ~~(see 2.2.1).~~  
262 Reports from ANEPC and the Portuguese Institute for the Sea and the Atmosphere (IPMA, ~~showing the fire plume evolution~~),

263 GNR and the Association for the Development and Industrial Aerodynamics (ADAI), were also used to identify fire arrival  
264 times and active firelines. Additionally, other data sources allowed ~~to the reconstruction of~~ wildfire spread, such as: the official  
265 wildfire time log (see 2.2.4)-, interviews (fire personnel involved in -suppression, local residents), field-work to identify the  
266 forward fire spread direction ~~based on scorched or charred foliage orientation~~, and other relevant data such as photos and  
267 videos. The fire spread isochrones were determined through spatial interpolation methods (spline and inverse distance  
268 weighting), on ~~high density~~high-density point clouds and experts' knowledge.

269  
270 Viegas et al., (2019) reconstructed the extreme wildfires of October 2017 based on fieldwork, interviews, photos/videos and  
271 information contained in the official wildfire time log. Since the fire progression data were not provided by the authors, here  
272 we used only very limited information regarding ignition location\time and general fire spread patterns, mostly to complement  
273 data provided by Guerreiro et al., (2017, 2018).

274  
275 ~~We chose to include these fire progressions in our database, because they represent the most extreme wildfires that occurred~~  
276 ~~in mainland Portugal, under persistent cloud cover conditions that limited hindered the June and October 2017 wildfires~~  
277 ~~progression mapping with the acquisition of satellite data.~~ Nonetheless, given the relevance of these wildfires we decided to  
278 include these fire progressions in our database because they represent some of the largest and most extreme wildfires that ever  
279 occurred in mainland Portugal. and for that reason they constitute relevant case studies, which otherwise would not be  
280 represented.

### 281 282 **2.3 Wildfire Progression (L1)**

283 Wildfire progression characterises the spatial and temporal evolution of the area burned in a specific fire event. ~~It also contains~~  
284 ~~information regarding the ignition time and location, as well as, flaming zones that correspond to active areas during the~~  
285 ~~wildfire. These include spot fires and reactivation/rekindling areas. In Portugal, a rekindle is a reactivation of the wildfire after~~  
286 ~~its official conclusion and is considered a new incident. For simplicity, we will consider rekindles as reactivations throughout~~  
287 ~~the rest of the manuscript.~~

288  
289 To ~~robustly~~ reconstruct wildfire progression, we combined the maximum available data from the different sources mentioned  
290 above, with the aim of obtaining convergence of evidence. This allowed reducing the limitations and uncertainties of each  
291 individual data source and building higher confidence in the derived wildfire progression.

292  
293 L1 data also contains information regarding the ignition time and location, as well as, flaming zones that correspond to active  
294 areas during the wildfire spread. These include spot fires and reactivation/rekindling areas. Combining all the available data-,  
295 we manually delimited the extent and time of the ignition, fire progression and active flaming zones of each wildfire. The

296 reconstruction was ~~always~~ made chronologically, i.e. starting from ignition and ending with the progression prior to wildfire  
297 containment. Sentinel-2 and Landsat 8/9 pre-fire images were used to identify areas burned shortly before the wildfire, and  
298 post-fire images were used to correct each progression polygon. As an example, Figure 3 shows how different data sources  
299 were combined to derive the spread of the Castro Marim (2021) wildfire. All wildfire progressions ~~items~~ (L1) were defined as  
300 polygons, each with a set of different attributes (explained below).

301  
302 **(Figure 3 near here)**

303  
304 Ignition location was defined as an area (vector polygon), instead of a point, to account for spatial uncertainties ~~in its location~~  
305 and to have a common data typology for the entire database, ~~in this case, vector polygons. To define ignition location w~~We  
306 used mostly official ~~ignition data, ignition location provided by first responders~~ and initial attack airborne photos ~~to define its~~  
307 ~~location~~. This was complemented with expert knowledge and information from fire personnel ~~to better define ignition location~~.  
308 For a small set of wildfires (mostly with nighttime ignitions), we also used satellite ~~imagery and~~ active-fire data to ~~identify~~  
309 ~~map~~ the approximate ignition ~~area~~ location. All ignitions were compared with later fire spread patterns and with the final burned  
310 area to reduce errors and guarantee consistency (e.g. ignition was contained in the final burned area). ~~Regarding ignition time,~~  
311 ~~the official time of alert was compared with high-15 min frequency MSG-SEVIRI FRP detections data,~~ to confirm the alert  
312 time or, in a very few cases, to anticipate the ignition time if energy was released before ~~the official ignition time. In addition,~~  
313 MSG-SEVIRI FRP data were also useful to identify (or confirm) the timing of reactivation(s). An clear example is shown in  
314 Figure 3, where the significant release of energy around 11:30, combined with ground data, allowed identifying the location  
315 and time of the reactivation zone.

316  
317 Active flaming zones were mostly derived from ground, airborne data and/or high spatial resolution satellite imagery.  
318 Alternatively, they were defined based on visual interpretation of multiple moderate resolution satellite imagery and often  
319 combined with active fire data (mostly VIIRS due to its higher spatial resolution). Inconclusive visual interpretations were  
320 discarded, as well as active zones that did not lead to any relevant subsequent fire spread. The ignition zone and all active  
321 flaming zones were always contained within the subsequent fire spread polygon.

322  
323 Wildfire progression was represented by a series of consecutive polygons delineating the temporal evolution of the area burned  
324 by the wildfire. The number of polygons depended on fire size and data availability. The progression polygons were built using  
325 as many data sources as possible, complementing each other in both space and time (see Figure 1). The variety of input data  
326 used have different associated uncertainties. When delineating the progression polygons priority was given to input data with  
327 higher spatial resolution, free from smoke and cloud contamination, and with the most complete view of the entire active part  
328 of the wildfire. Typically, the first priority level data (i.e. highest confidence) were Sentinel-2 and Landsat 8/9 images, and  
329 AVRAC aeroplane photos/videos. The second priority level was composed of ground data, VIIRS active-fires, PROBA-V and

330 Sentinel 3 images (both at 300 m resolution) and helicopter photos/videos. The third priority level were images and active-fire  
331 data from moderate resolution satellites (MODIS and Sentinel 3). The fourth, and last priority level (i.e. lowest confidence)  
332 were composed by FRP data from MSG-SEVIRI and the official wildfire time logs. The data from the large 2017 wildfires  
333 reports were handled separately. The progression polygons from Guerreiro et al., (2017, 2018) were deemed as high confidence  
334 data and were complemented with data and information from Viegas et al. (2019) and, at times, with satellite data.

335  
336 A common challenge found in the delineation of the wildfire progression were the uncertainties associated with the correct  
337 time an entire progression polygon burned. These uncertainties were present in almost all data sources. For example, a polygon  
338 derived by fire operatives on the ground could have stopped burning minutes or hours before data collection. Additionally,  
339 satellite active-fire data can depict areas that are hot minutes or hours after the fire front stopped progressing. The strategy to  
340 minimize such uncertainties was to use data from multiple sources, seeking convergence of evidence. As an example:-, a  
341 common feature found in the data was ~~a pronounced-substantial~~ fire spread during daytime, followed by very limited nighttime  
342 progression. In these cases, first, the nighttime fire progression was delineated using active fire data (mostly VIIRS) and  
343 complemented with ground data, when available. Second, satellite and/or airborne imagery acquired during the following  
344 morning were used to perform any necessary adjustments in the nighttime spread polygon(s). ~~Satellite-derived~~ FRE estimates  
345 ~~based on of~~ MSG-SEVIRI/MSG were also used to identify if any substantial fire activity occurred between VIIRS/MODIS  
346 nighttime overpass and daytime imagery (satellite and/or airborne). We assumed that fire activity decreased significantly when  
347 the wildfire released less than 0.5 TJ per ~~30-30 min~~ period, and anticipated the date/hour of the fire spread polygon accordingly.  
348 In smaller wildfires (<500 ha) this threshold was set to 0.1 TJ. ~~These-Such~~ thresholds were defined empirically (see Discussion  
349 section). The entire procedure reduced the uncertainties associated with the ~~delineation of the nighttime spread~~  
350 ~~polygons~~ definition of the end date/time of the progression polygons. It should be noted that the fire behaviour within the time  
351 span of each progression polygon was unknown and, therefore, it was assumed to be free burning ~~in a homogeneous way at a~~  
352 constant rate (Storey et al., 2021). When data were insufficient to determine when a given area burned, the spread polygon  
353 was flagged as “uncertain”.

354  
355 Ignitions/active flaming zones were linked to the resultant spread polygon(s), by assigning a numeric label to a field called  
356 “zp\_link”, providing an explicit connection between both, and allowing to track the source of a given ~~burned~~-progression  
357 polygon. When information was insufficient, for example, the start of the progression polygon was unknown, zp\_link was  
358 ~~defined set as to~~ “0”. After all ignition(s), fire progressions and active flaming zones were defined, each wildfire was divided  
359 into burning periods. We assumed that each burning period contained relatively homogeneous fire runs that:

- 360
- 361 i) were ignited by the same set of ignitions or active flaming zones;
- 362 ii) did not exhibit large fire spread direction shifts (less than 45° of variation);
- 363 iii) were not impeded by barriers (e.g. previously burned area) and;

364 iv) did not exhibit significant changes in fire behaviour (e.g. large ROS variation).

365  
366 Regarding the latter criterion, for example daytime and nighttime runs were usually separated in different burning periods even  
367 if criteria (i)-(iii) were fulfilled. By definition, a new active flaming zone always marked the beginning of a new burning  
368 period; however, not all burning periods started with an ignition or active flaming zone, since this depended on data availability.

369  
370 When direct evidence of fire spotting was available (i.e. exact location/timing of the spot fire(s), typically from ground and/or  
371 airborne data), if the fire front(s) rapidly (under 1 hour) coalesced with the original fire front, fire progression was merged  
372 into a single polygon. In the remaining cases, typically associated with medium distance spotting and/or slow burning fire  
373 fronts, the spotting location was defined as a new active flaming zone setting, defining a new burning period. When the exact  
374 location/timing of the spot fire was not available, evidence of spotting consisted of observations of non-contiguous burned  
375 areas that resulted from the same wildfire. These were typically separated by rivers, lakes and settlements. In these cases, due  
376 to lack of data, the polygons separated from the major fire run were defined with zp\_link=0 if the distance was larger than 200  
377 m. No fire behaviour descriptors were calculated for these ~~burned-areas~~polygons.

378  
379 The definition of the burning period was always dependent on data availability and, in some cases, was subjective. For the  
380 progressions derived using only satellite data, the length of the burning period was mostly determined by the timing of the  
381 satellite overpass(es) and ~~the-FRE's~~ temporal evolution. For the progressions derived from more detailed data, the above-  
382 mentioned criteria were easier to fulfil. In a few cases, uncertainties in fire progressions led to slightly overlapping periods.  
383 An example is shown in the Results section and implications are addressed in the Discussion section.

384  
385 After collecting input data for a large number of wildfires, only those with at least one valid progression and ~~a valid~~  
386 ignition/active flaming zone were kept. We eliminated all suspicious cases where uncertainties were large, for example, due  
387 to the presence of persistent smoke or clouds in the satellite/airborne images or absence of valid ground data. The L1 wildfire  
388 progression database was defined by a set of polygons with attribute fields (details in section 35). The date/hour of each  
389 ignition(s), fire spread and active flaming zones (if applicable) were approximated to the nearest 30 min<sup>2</sup> period. Fire  
390 progression data from external reports were adapted to the rationale of the fire database described above. ~~Findings from~~  
391 ~~different reports for the same wildfire were compared and satellite data was used to complement and improve the original fire~~  
392 ~~progressions.~~

## 394 2.4 Wildfire behaviour (L2)

395 ~~The estimation of fire~~ Fire behaviour descriptors ~~was were estimated using supported by the use of~~ spatial graphs. A graph is  
396 a mathematical structure composed of nodes (N) and edges (E), which connect the nodes (Dale and Fortin, 2010). Based on

397 the fire spread polygons (L1) (Figure 4a), we built a spatial directed graph (or digraph) where each node refers to a spread  
398 polygon, and each edge connects two spread polygons (i.e nodes), with a valid link (i.e.  $zp\_link > 0$ ). These two nodes burned  
399 at different times, one earlier ( $t_i$ ) and the other later ( $t_j$ ). The value of each edge was defined as the time elapsed between two  
400 nodes ( $\Delta t_{ij}$ ) (Figure 4b). A node can have an inward edge (where fire is being transmitted from) and an outward edge (where  
401 fire is being transmitted to).

402  
403 First, the nodes were connected only if the associated fire progression polygons were contiguous, had the same  $zp\_link$  value  
404 and burned at different timings. Second, only the edges corresponding to the shortest elapsed time between two nodes were  
405 kept. The digraph allowed to formally structure the connections between fire spread polygons, enabling the calculation of fire  
406 behaviour descriptors.

407  
408 To allow for a better understanding of the methods used, a brief explanation based on the Ourique (2019) wildfire is provided.  
409 In Figure 4, the number of the polygons on the left matches the number of nodes on the right. After its start (1), the wildfire  
410 spread fast to the south and burned the area delimited by polygon 2 in about 120 min<sup>2</sup>. Fire behaviour changed after the head  
411 run, and the left flank became the head and subsequently made a run to the southeast, burning the area represented by polygons  
412 4, 5, 6 and 7, in about 180 min<sup>2</sup>. This fire behaviour change observed at  $t=120^2-120\ min$  determined the definition of two  
413 burning periods: one corresponding to the initial head run, the other corresponding to head run from the left flank. The digraph  
414 was built with 7 nodes and 6 edges with values ranging between 30<sup>2</sup>-30min and 120<sup>2</sup>120 min.

415  
416 **(Figure 4 near here)**

417  
418 Based on the fire progression (L1) and the corresponding di-graph, we calculated the following set of fire behaviour descriptors  
419 (L2): forward ROS (m/h), direction of forward spread direction-(° from North), FGR (ha/h), and FRE (TJ). The polygons  
420 referring to areas burned shortly before the fire analysed were removed from L2.

421  
422 ROS was calculated for each node ( $N_j$ ) with a valid inward edge ( $E_{ij}$ ) connecting it to a prior node ( $N_i$ ). By definition, the  
423 forward ROS refers to the head of the fire and was calculated considering the longest distance line connecting two consecutive  
424 fire progression polygons (i.e. nodes). representing the fastest spread (Storey et al., 2021). The ground distance ( $D_{ij}$ ) between  
425 each pair of polygons was calculated as follows:

- 426
- 427 • All ground distances between the polygon vertices of  $N_i$  and  $N_j$  were calculated, using the European Digital Elevation  
428 Model (EU-DEM v1.1, <https://land.copernicus.eu/imagery-in-situ/eu-dem/eu-dem-v1.1>) resampled to 50 m spatial  
429 resolution;

- 430 • For each vertex of the  $N_j$  polygon, only the shortest distance was kept and the corresponding pair of vertices, from  
431  $N_i$  and  $N_j$ , were stored;
- 432 •  $D_{ij}$  was defined as the maximum of all shortest distances between vertices.

433  
434 The ROS was calculated by dividing the distance ( $D_{ij}$ ) by the time elapsed between the pair of polygons ( $\Delta t_{ij}$ ) and expressed  
435 in m/h. We divided the ROS calculation in two distinct measures:

- 436  
437 • Partial ROS (hereafter, ROSp) calculated between two consecutive polygons;
- 438 • Mean ROS (hereafter, ROSi), calculated between the ignition (or active flaming front) and a given spread polygon.

439  
440 The spread direction was calculated using trigonometric rules considering the two above-mentioned vertices between two  
441 polygons. The spread direction was calculated both for ROSp and ROSi, where the difference lies only on the origin polygon.  
442 FGR was calculated dividing the burned area by each polygon/node ( $A_j$ ) by the time elapsed between polygons ( $\Delta t_{ij}$ ) and was  
443 expressed in ha/h. An example of the calculation of these fire behaviour descriptors is shown in Figure 5.

444  
445 **(Figure 5 near here)**

446  
447 In addition to the standard fire behaviour descriptors, we also estimated the FRE for each progression polygon. This procedure  
448 raised additional challenges. First, MSG-SEVIRI is affected by clouds and smoke, which can hinder the estimation of FRE for  
449 some periods of the wildfires, or for their entire duration. Second, due to the coarse resolution of MSG-SEVIRI it was not  
450 possible to calculate the FRE for each polygon directly. To circumvent this, FRE was calculated for each 30 min<sup>2</sup> bin from  
451 ignition until the date/hour of the last wildfire spread polygon. In parallel, we estimated the area burned in each spread polygon  
452 every 30 min<sup>2</sup>, using its start/end dates and assuming a constant FGR. Then, for each 30 min<sup>2</sup>-bin, the total FRE was divided  
453 by weighting its value by the proportion of area burned in each spread polygon. Finally, for each spread polygon the 30<sup>2</sup> min  
454 FRE estimates were summed only if they covered ~~more~~ more than 70% of its duration ( $\Delta t_{ij}$ ), to ensure that the total FRE was  
455 representative.

456  
457 We also estimated the FRE flux rate ( $\text{GJ ha}^{-1} \text{h}^{-1}$ ) for each spread polygon by dividing the estimated FRE by the corresponding  
458 burned area extent and its duration ( $\Delta t_{ij}$ ). As FRE is highly dependent on the extent burning ~~at-in~~ a given time window, the  
459 FRE flux rate can provide estimates closer to “instantaneous” values ~~required-useful~~ for other applications.

## 460 2.5 Simplified Wildfire behaviour (L3)

461 We calculated simplified metrics representing a mean fire behaviour across each burning period. This enables higher-level  
462 analysis of the data, but at the cost of losing detail and making simplifications to the calculation of the fire behaviour metrics.  
463

464 The simplified ROS corresponded to the ROS<sub>i</sub> estimated for the last spread polygon of a given burning period i.e., the average  
465 ROS between the start and the end of each burning period. FGR was defined as the sum of the area burned in the period divided  
466 by its duration. The total FRE was calculated considering all energy released by the polygons burning within the burning  
467 period, if FRE estimates covered more than 70% of the area burned.

## 468 2.6 Quality Control and Quality Assurance (QC/QA)

469 All L1 to L2, and L2 to L3 processing was done using Matlab scripts complemented with quality controls checks to identify  
470 errors in the original L1 data. These included simple checks to incorrect field names, incoherent data format (e.g., date/hour),  
471 and consistency on the fire spread structure defined by the di-graphs, as for example: i) time elapsed between node was always  
472 positive;and ii) every spread polygon with ~~a positive~~-zp\_link>0 was always associated with a predecessor valid node (either  
473 of “z” or “p” type), among others.

474  
475 During the processing of L1 data to L2, we did frequent quality checks to identify potential errors, for example, null values of  
476 ROS or FGR associated with valid fire spread polygons, fire progression polygons that did not have a known start/end date, or  
477 did not have a known link to a preceding fire source (e.g., active flaming zone). In addition, we selected some wildfires, ~~and~~  
478 made independent calculations of the ROS and FGR and compared them with ~~the ones~~those estimated using the ~~developed~~  
479 Matlab code ~~developed~~. All these quality control steps assured that the data produced were reliable and of the best possible  
480 quality. The process was iterative, requiring frequent corrections to the L1 data and ~~the re-running of~~the quality check.

481  
482 Finally, for each wildfire, we defined a confidence flag that provides an overall information of ~~the how-reliability of~~ the  
483 ~~estimated fire~~-progression data-were. Although directly related to L1, ultimately it should also provide the user an estimate of  
484 the confidence associated with L2 and L3. This was defined empirically, based on the uncertainties that arose in the process  
485 of building the fire progression polygons and was graded into a 5-level system where 1 refers to the ~~lower-lowest~~ quality and  
486 5 to the highest quality (Table ~~A+A2~~).

## 487 3 Results

### 488 3.1 Overview of the PT-FireSprd database

489 The PT-FireSprd database contains data for 80 large wildfires that occurred between 2015 and 2021. The individual wildfire  
490 burned area extent ranges from 250 to 45,339 ha, with a mean and median area of 5,990 and 1,665 ha, respectively. The 80  
491 wildfires were distributed throughout mainland Portugal, covering a wide range of environmental conditions (Figure 6). The  
492 database spans a wide fire behaviour variability both between (e.g. Figure 6A, B, F) ~~as well as~~ and within each wildfire (e.g.  
493 Figure 6C, E, D). The total burned area extent of the wildfires contained in the database ~~was~~ is around 460,000 ha, which  
494 represents about half of the area burned in the 2015-2021 period. On average, progression was reconstructed for 93% of the  
495 area burned by the 80 wildfires, leaving 7% deemed “uncertain”. Wildfire behaviour descriptors were estimated for 88% of  
496 the burned area extent (ca. 400,000 ha). The time elapsed between two consecutive fire progression polygons ranged between  
497 30 min<sup>2</sup> and 14h30m with an average value of 3h15m. The mean duration of the burning periods was around 8h00m, with a  
498 standard deviation of 4h50m.

499

500 **(Figure 6 near here)**

501

502 A total of 1,197 polygons with ROS and FGR estimates (L2) were derived from the progression data. We excluded very small  
503 polygons (<25 ha) from further analysis, resulting in a dataset with 874 observations. ~~Out of~~ the 1,197 polygons, ~~only~~ 609  
504 had FRE estimates. Regarding L3 data, ROS and FGR were calculated for 241 burning periods (L3) and total FRE was ~~only~~  
505 estimated for 162 burning periods.

506

507 Overall, confidence in the database was lower for the earlier years (2015-2016) because input data ~~was~~ were mostly from  
508 existent satellites. In 2017, the quality increased due to the integration of: i) ground data; and ii) data from 2017 large wildfires  
509 ~~external reports that analysed the extreme wildfires of June and October~~. From 2018 onwards, the integration of the monitoring  
510 ~~aeroplanes/aircrafts~~, the creation of the FEBMON system, and the rapid availability of all the data that flows through it,  
511 significantly improved confidence of the derived fire progressions.

512

513 The estimated forward ROS displayed a long-tail distribution (Figure 7, in log-scale) with a median value of 341 m/h and  
514 average ROS of 746 m/h, representing large variability (std = 1071 m/h, cv = 143%). About 20% of the ROS values were  
515 larger than 1,000 m/h and about 9% were larger than 2,000 m/h. The maximum observed ROS was ~~8956~~ 8,900 m/h in the  
516 Lousã wildfire of October 2017. The FGR distribution was highly skewed towards low values, with median and average values  
517 of 40 ha/h and 191 ha/h, respectively (sd = 438 ha/h, cv = 228%). About 10% of the observations had FGR larger than 500  
518 ha/h and only about 5% were larger than 1,000 ha/h. The maximum observed FGR was ~~4,400~~ 36 ha/h in the Pedrogão Grande  
519 wildfire ~~of June (2017)~~.

520

521 **(Figure 7 near here)**

522

523 The ROS distributions of the L2 and L3 datasets were similar. The largest differences were located in the lower and upper  
524 tails, where the L3 ROS tends to be smoother due to the averaging procedure done over a longer time span. The FGR  
525 distributions for L2 and L3 were also very similar, probably because all the polygon areas within a burning period are summed,  
526 and the value does not result from an average. Differences were larger for more complex wildfires, for example with “finger  
527 runs” (e.g. areas resulting from rapid propagation in a different direction than the dominant fire front, often related with wind  
528 shifts).

529

530 We compared the histograms of L2 ROS and FGR for three aggregated confidence levels. The distribution of ROS estimates  
531 for wildfires with lower confidence was slightly skewed towards lower values, when compared with higher confidence  
532 estimates (Figure B1). The ROS distributions peaked at 200 m/h, 500 m/h and 800 m/h for very low/low, moderate and  
533 high/very high confidence, respectively, showing a clear relationship between confidence and estimated ROS. Regarding FGR,  
534 very high values above 500 ha/h were prevalent in wildfires with high and very high confidence progressions (Figure B2).  
535 Results are similar if data from external reports for the extreme wildfires from June and October of 2017 are not included.

536

537 Estimated ROS and FGR were compared and percentiles 25, 50, 75, 90 and 97.5 were calculated separately for each variable  
538 independently (Figure 8). The percentile values were simplified to enable a clear communication of results, especially between  
539 researchers and fire personnel. ~~The percentiles were translated into empirical classes, ranging from “very low” to “extreme”~~  
540 ~~fire behaviour.~~ In general, as ROS increases so does the FGR. However, the relationship between ROS and FGR depends on  
541 the morphology of the fire perimeter: elongated fast-spreading wildfires had relatively higher ROS and lower FGR (e.g. Figure  
542 6B, C), and while more complex burned area perimeters had relatively lower ROS and higher FGR (e.g. a flank run with an  
543 extensive active fireline; see Figure 6A and the last polygons of Figures 6E and 6F). The dispersion data scatter tends to  
544 increase with higher ROS/FGR values, suggesting a progressively larger dependence on the burned area extent/perimeter.  
545 Identification of the drivers factors determining behind such relationships is beyond the scope of this work. Nevertheless,  
546 wildfires at the extreme of the distribution with “Extreme” behaviour had both very high ROS and FGR values ~~of ROS and~~  
547 ~~FGR~~.

548

549 **(Figure 8 near here)**

550

551 Burned area extent is a relevant fire behaviour descriptor for researchers and fire management personnel. Analysis suggests  
552 shows that the area burned by a wildfire is mostly determined by its FGR ( $r=0.84$ ) rather than by the speed of the forward

553 spread ( $r=0.62$ ; Figure 9a,b). The (cor)relations were lower using L2 data. As expected, FRE is highly correlated with burned  
554 area extent ( $r=0.85$ , Figure 9c), ~~and consequently of FGR~~. Correlation between ROS and average rate of energy release ( $\text{TJ}/\text{h}$ )  
555 is lower ( $r=0.30$ , Figure 9d), ~~however although~~, there is a general direct relation between both descriptors.

556  
557 **(Figure 9 near here)**  
558

### 559 **23.2 Case study: The Castro Marim 2021 wildfire**

560 Here, we describe in detail the progression and behaviour of a specific wildfire to show how the PT-FireSprd database can be  
561 used, for example, to analyse case studies, ~~something which is~~ often done by researchers and fire analysts.

562  
563 The Castro Marim wildfire burned 5950 ha on the 16th and 17th of August of 2021. Figure 10 shows its reconstructed  
564 progression (a) and associated ROS (b). Ignition occurred at nighttime (01:00) and a single run occurred towards SE until  
565 approximately 08:30, defined as the first burning period. The mean ROS was 618 m/h, ranging between 321 and 957 m/h  
566 (Figure 10c). The estimated FGR for the burning period was 43 ha/h, ranging between 33 and 77 ha/h, and the total FRE was  
567 13 TJ (Figure 10d).

568  
569 **(Figure 10 near here)**  
570

571 Fire progression halted for about 3h until the wildfire reactivated around 11h30. It spread southwards until the head stopped  
572 in an agricultural area around 19h30. In this second burning period, fire behaviour was significantly different from the first.  
573 The mean ROS was ca. 1,500 m/h, reaching a maximum value of 3,720m/h between 16:30 and 17:30. On average, ~~the fire~~  
574 grew at a rate of 455 ha/h, however, significant variability was observed with values reaching 1,236 ha/h coinciding with the  
575 ROS peak. ~~Framing the fire behaviour descriptors with the empirical classes represented in Figure 8, t~~The behaviour in the  
576 second burning period was often ~~framed in the “Very High” class, i.e.~~ between percentiles 90 and 97.5. As a consequence of  
577 the behaviour exacerbation, the wildfire released around 38 TJ, with peaks of about 9 and 12 TJ observed during the afternoon.  
578 The energy flux rate was highest between 16:00 and 16:30, coinciding with an abrupt increase in ROS (Figure 10d).

579  
580 After the fire head stopped, a secondary head run stopped around 23:00 in a previously burned area (burning period 3). In the  
581 follow-up, two left flank runs were observed, one until 02:30 and the other one, resulting from a reactivation, until 06:00, with  
582 decreasing ROS, FGR and FRE. A secondary peak in the energy flux rate was estimated around 0:00, associated with an  
583 increase in ROS and FGR.

585 Finally, in the Castro Marim wildfire, burning periods 3 and 4 overlapped in time. A progression polygon in the rear/right  
586 flank was delimited by fire personnel at 02:30, however the prior contiguous progression was identified at 16:30, suggesting  
587 a very low burning flank, opposite to the fast burning part of the wildfire southwards. This overlap had no effect on the average  
588 ROS, and only a very slight effect on the estimated FGR and FRE. However, users must be aware that burning periods seldom  
589 overlap (~4% registered in the entire dataset), which may have implications in ~~posterior-subsequent analysis~~analyses.

## 590 4 Discussion

### 591 4.1 The PT-FireSprd database

592 The PT-FireSprd is the first open access fire progression and behaviour database in the entire Mediterranean Europe. The  
593 progression of 80 large wildfires that occurred in mainland Portugal between 2015-2021 is reconstructed and fire behaviour  
594 descriptors such as ROS, FGR and FRE are estimated, dramatically expanding the extant information (Palheiro et al., 2006;  
595 Rodriguez y Silva & Molina-Martínez 2012; Fernandes et al., 2016). Wildfire progression was derived by converging evidence  
596 from multiple data sources, which provides added ~~credibility-reliability~~ to the database. Wide variability in fire behaviour is  
597 covered, tackling an important limitation pointed out by Cruz (2010). The approach presented will be used to update the  
598 database in the following years for Portugal, and can be replicated in other countries, depending on data availability.

599  
600 The large number of fire behaviour observations, both at the polygon level (L2) and at the burning period level (L3), provide  
601 enough information for a wide variety of potential applications. Combined with detailed information on the drivers, namely  
602 weather and fuel, and effects. ~~For example,~~ it can be used to: i) improve current knowledge on the drivers affecting the  
603 behaviour of large wildfires; ii) calibrate existing or new models which ultimately should help to better predict fire behaviour  
604 and support efficient fire management strategies (Alexander and Cruz, 2013a); iii) support the construction of case studies by  
605 fire analysts and contribute to better training of fire personnel (Alexander and Thomas, 2003); iv) contribute to improve  
606 operational fire suppression strategies; v) better understand how fire behaviour is linked to its effects (Collins et al., 2009),  
607 ~~and~~ v) improve fire danger rating (Wotton, 2009); and vi) better characterize fire regimes (Pereira et al. 2022). In addition, the  
608 fire behaviour classes described in Figure 8 can assist fire suppression operations, including resources dispatching and  
609 decisions to fight or flee, or offensive vs defensive strategies.

610  
611 For several reasons, it is easier to collect information for larger wildfires than for smaller ones. The wide range in fire sizes  
612 ~~present~~ in the PT-FireSprd database suggests that it is representative of wildfires burning under a broad range of conditions.  
613 However, smaller wildfires (between 100 and 500 ha) are slightly under-represented in the database creating a potential bias.  
614 This can be particularly relevant if one considers the high proportion of smaller wildfires that occur every year. Thus, fire  
615 behaviour descriptors may also be biased towards larger values ~~which-that~~ may have an implication, for example, on the  
616 calculated fire behaviour ~~classes-percentiles (defined in~~ Figure 8). Note that for typical fuel loads, say 15-20 t ha<sup>-1</sup> (Fernandes

617 et al., 2016), ~~the third class in ROS between percentiles 50 and 75 Fig. 8~~ already corresponds to fires that are very difficult to  
618 control ~~directly~~ (Hirsch and Martell, 1996). ~~Nevertheless, these classes should be considered as a~~ The ROS and FRR historical  
619 distribution are a first ~~exploratory~~ approach with the aim of creating a simple and clear communication baseline between  
620 researchers and fire personnel based on quantitative fire behaviour data. Ultimately, the database will allow framing the  
621 behaviour of new wildfires according to historical patterns. Adding smaller wildfires to the PT-FireSprd database will certainly  
622 help to better represent a wider range of fire behaviour patterns.

623  
624 Confidence in the wildfires of 2015-2016 was lower than for the most recent ones due to relevant advances in operational fire  
625 monitoring, resulting in better quality and higher quantity of fire data. Since 2018, the FEBMON system has improved and  
626 grown, providing larger quantity and higher quality data, thus leading to more reliable and detailed fire progression  
627 reconstructions. The distribution of the duration of the spread polygons between 2015 and 2021 (Figure B3) shows  
628 heterogeneity of the database across time, but also the evolution introduced ~~by the implementation of along with the~~ FEBMON  
629 ~~system~~. Results suggest that ~~estimates of~~ ROS and FGR ~~might may~~ be underestimated predicted in wildfires with lower  
630 confidence, most probably due to the lack of data to thoroughly cover the afternoon, but especially the early night period (i.e.  
631 between VIIRS/MODIS day and nighttime overpasses, Figure 1). This issue is further discussed in section 5.2. The user must  
632 take into account the characteristics of the database and can choose to use the entire or part of the dataset based on the  
633 confidence flag or year of the wildfire.

634  
635 The PT-FireSprd database is flexible and open, allowing the users to subset the data based on their needs and requirements.  
636 For example, users can decide to work with fire behaviour descriptors at the polygon level (L2) or at the burning period (L3),  
637 or can create their own subset depending on their objectives. The dataset is heterogeneous which is reflected in two main  
638 components: the duration of the spread polygons and the burning periods, and the confidence flag associated with each wildfire.

639  
640 Regarding the duration, the average time elapsed between two progression polygons was 3h30 (L2) and 8h15 for the burning  
641 periods (L3). Durations were large in 2015 and 2016 (median values above 9h), decreased significantly in 2017 with the  
642 integration of hourly isochrones from Guerreiro et al., (2017, 2018), and ~~have~~ had median durations below 2h since 2019  
643 (Figure B3). Gollner et al., (2015) argued that fire progression observations need to be made in real-time with a 10-~~metre m~~  
644 spatial resolution every 10 min<sup>2</sup> to meet the needs of fire behaviour forecasting. However, in operational context the current  
645 objective is to predict fire behaviour time intervals larger than or equal to 30 min<sup>2</sup> (Cruz and Alexander, 2013). Considering  
646 the average duration of the burning periods, that represent a single fire run, the average time elapsed between progression  
647 observations represents a good compromise and a clear advance in current data. Regardless, users can subset the database  
648 based on the duration of either the progression polygons or the burning periods. L3 descriptors can be useful to provide more  
649 homogeneous and normalised fire behaviour descriptors, dampening the effect of the large variability in L2 durations,  
650 allowing, for example, a better comparison between wildfires.

651

652 Finally, ~~preliminary~~ results suggest that considering both ROS and FGR can improve understanding of wildfire dynamics. The  
653 relation between both ~~is related to~~ is dependent on perimeter morphology and extent (among others), and future work is needed  
654 to better understand the underlying factors. Most importantly, FGR was a better explanatory variable of burned area extent  
655 than ROS. The practical consequence is that large burned areas can be generated by wildfires with a moderate forward ROS  
656 but with large FGR ~~of the entire perimeter~~, which in turn is highly influenced by spread duration and perimeter extent. This  
657 should have implications for both the research and operational communities. FRE was estimated for a lower number of spread  
658 polygons and burning periods when compared with ROS and FGR. This was most likely due to the impact of clouds and smoke  
659 on MSG-SEVIRI detections and the ~~relatively~~ conservative minimum number of observations threshold (75%). FRE and  
660 burned area extent were closely related, however, relations between FRE and ROS were poor/moderate. One of the possible  
661 reasons may be related with the need to consider the effect of the active perimeter extent when comparing both descriptors.

## 662 **4.2 Limitations and future improvements**

663 The generic limitations of the input data have been thoroughly described in Section 1. In particular, for Portugal some  
664 limitations of the data must be pointed out. Fire progression perimeters and fire points collected in the ground by fire personnel  
665 have relevant spatio-temporal uncertainties. For example, there is often a lag between the date/hour a polygon is drawn in the  
666 ground and the actual date/hour it burned completely. Another relevant issue is that of data acquisition / reporting errors done  
667 by fire personnel, which may be reduced by improved training and experience. The number of users of the FEBMON system  
668 has been growing in recent years and, with adequate training, it is expected that the quality and quantity of ground data will  
669 increase in upcoming years. In fact, over 27,000 aerial and 2,500 ground photos were taken in the year of 2022, which  
670 represents a relevant increase compared to previous years.

671

672 Regarding airborne data, the discussion ~~can~~ may be separated into two components. First, initial attack photos, which can be  
673 extremely useful to draw initial fire progression and infer probable ignition areas, are not collected for every wildfire to which  
674 a helicopter is dispatched, and sometimes are of poor quality. Additional training and increasing the awareness of fire personnel  
675 for the relevance of the data they collect is necessary. Second, ~~aeroplane~~ aircraft data are acquired at relatively low altitude,  
676 precluding a synoptic view of the wildfire. Time lags between data acquisition for different parts of the wildfire (e.g. left vs.  
677 right flanks) may be large and introduce relevant spatio-temporal uncertainties in the delineation of the fire progression. In  
678 addition, perimeters are drawn manually and depend on the training and experience of the fire expert. In upcoming years, the  
679 integration of new airborne sensors, specially with multispectral capability, the ability to perform high-altitude scans and the  
680 use of automatic perimeter delimitation procedures (e.g., Valero et al., 2018) should improve data quality and reduce the time  
681 lags of airborne fire observations. With this new capacity, it will be possible to integrate deep learning processes in the data  
682 analysis, increasing both the quantity and quality of the available fire data. This integration will also allow a well-organised

683 structure in data collection, management and analysis, improving decision-support systems. Finally, the use of UAVs during  
684 nighttime (pioneered in 2022 in Portugal) will complement aeroplane/helicopter data during periods of low data availability.

685

686 Regarding official fire data, errors in the delineation of ~~final~~ burned area perimeters and in the ignition location, often located  
687 outside of the fire perimeter, need to be corrected to increase the quality of the PT-FireSprd database. ~~Regarding satellite data,~~  
688 ~~implementing~~ Implementation of (semi-) automatic algorithms to delimit fire perimeters using satellite data (e.g., Chen et al.,  
689 2022) will increase ~~the data~~ availability ~~of fire perimeters~~ and reduce the uncertainties associated with manual perimeter  
690 ~~delineation~~ delineation. Improvements in the spatial resolution geostationary satellites, such as the recently launched Meteosat  
691 Third Generation (MTG), will certainly improve fire behaviour estimates, as already observed in HIMAWARI-8 and last  
692 generation GOES satellites.

693

694 ~~Regarding~~ Concerning methodological uncertainties, the major challenge was to assign the correct date/hour to a specific  
695 burned area. For example, when raw data sources indicated that an area burned but active areas were absent or small, there  
696 were always uncertainties as to when it actually burned completely, which ~~could~~ may lead to a relevant ROS/~~growth rate~~ FGR  
697 underestimation. These uncertainties were larger between dusk until VIIRS overpass(es) and between the later and dawn. One  
698 approach to reduce these uncertainties was to use FRE data to monitor the daily cycle of fire activity and help to better define  
699 the start/end date of a progression polygon. The method was empirical and future work is needed to better define the thresholds  
700 for setting the ignition or reactivation times, as well as the end of a fire progression. Exploratory analysis done in a few  
701 wildfires of the PT-FireSprd database suggest that FRE has a significant drop after the head of the fire stops, which may take  
702 several minutes/hours until reaching the FRE thresholds used. This moment is commonly accompanied by ~~a~~ flank growth that  
703 burns slower and releases lower amounts of energy. ~~These~~ Such fire dynamics probably explain why ROS was likely  
704 underestimated in low confidence wildfires and why FGR was less affected by data confidence. Improvements can be achieved  
705 in the future, through the use of more sophisticated methods (e.g. change point detection), more ground observations during  
706 the head to flank run transition, and higher spatial resolution data from geostationary satellites. Part of these improvements  
707 can be used to partially update the 2015-2021 wildfires of the PT-FireSprd database.

708

709 In terms of characterising uncertainties and its effects, future work should also adopt a metrological approach to propagate  
710 uncertainties to the descriptors, providing useful information to users. By providing an uncertainty assessment, the PT-FireSprd  
711 database would be on the pathway ~~of to~~ Fiducial Reference Measurement (FRM) compliance (Niro et al. 2021).

712

713 The continuous update of the PT-FireSprd database will require a joint effort by researchers and fire personnel. The automation  
714 of data collection procedures (discussed above), as well as dedicated training to fire personnel, are key factors to guarantee  
715 both the quality as well as a sustainable update of the database. In ~~the~~ upcoming years, other fire behaviour descriptors ~~could~~  
716 may be included such as type of spread (surface vs. crown fire), fireline intensity, flame ~~size~~ length, spotting (including

717 maximum distance) and/or PyroCb occurrence. Finally, methods described in the current work can be, at least partially, [be](#)  
718 applied to many other fire-prone areas of the globe and contribute to the much-needed data on observed wildfire behaviour.

## 719 **5 Data Availability**

720 The dataset contains generic metadata file with relevant information for each wildfire (Table [A2A3](#)), such as the fire ID,  
721 official incident ID (ANEPC, 13 digit number), fire name, municipality, civil parish, start date, duration (hours), extent (ha),  
722 among others. The fire name was defined as Municipality\_DDMMYYYY, where DD is day, MM month and YYYY the year.  
723 In case [that](#) more than one wildfire occurred in the same municipality on the same day, we added an additional string at the  
724 end of the fire name (e.g. “\_2”).

725  
726 The dataset is then divided in 3 Levels, [with three in the](#) corresponding folders:

- 727 • Fire Spread (L1): Each year has a separate folder that contains one folder per wildfire [labeled](#) with the fire  
728 name. It contains a polygon shapefile with the attributes listed in Table [A3A4](#).
- 729 • Fire behaviour (L2): A single polygon shapefile that contains all wildfires and estimated fire behaviour metrics for  
730 each individual fire spread polygon. The attributes are listed and explained in Table [A4A5](#).
- 731 • Fire behaviour (L3): A single polygons shapefile that contains the simplified fire behaviour metrics calculated for  
732 each burning period. The attributes are described in Table [A5A6](#).

733  
734 The generic metadata is connected to L1 data through the “[fire name](#)” field, and to L2 and L3 through the fire “ID” field.  
735

736 The data are freely available at <https://doi.org/10.5281/zenodo.7495506> (last access: 30th December 2022; Benali et al. 2022).  
737 We intend to update the database annually with wildfires from the current fire season and implement continuous improvements  
738 to the procedure. Also, if additional information from past wildfires becomes available, we will update the database either by  
739 changing existing fire spread polygons or by adding new wildfires. Updates for future years depend on the availability of input  
740 data and associated funding.

## 741 **6 Conclusions**

742 The Portuguese Large Wildfire Spread Database (PT-FireSprd) is the first open access fire progression and behaviour database  
743 available within Mediterranean Europe. It includes the reconstruction of the progression of 80 large wildfires ([>100 ha](#)) that  
744 occurred in [mainland](#) Portugal between 2015 and 2021, [that which](#) was derived by [seeking](#) converging evidence from multiple  
745 data sources, ~~which provides added credibility to the database~~. PT-FireSprd contains a very large number [estimates](#) of key fire  
746 behaviour [observations](#) descriptors, such as ROS, FGR and FRE. Based on the statistical distribution of ROS and FGR, we

747 defined 6 ~~percentile intervals broad fire behaviour classes~~ that can be easily communicated to both research and management  
748 communities and to support a wide number of applications, including better fire management strategies. The PT-FireSprd has  
749 a large potential to contribute to the development of better fire behaviour prediction tools, improve our current knowledge on  
750 wildfire dynamics, foster better operational training and contribute to ~~better-improve~~ decision-making. The approach will be  
751 used to continuously update the database in the following years for Portugal and can be replicated in other countries/regions,  
752 depending on data availability. Improvements in data quality and the implementation of automated methods are key factors  
753 for the regular update of the PT-FireSprd database in the future.

## 754 **Appendix A: Supporting material for the Methods**

755 (Table A1, Table A2, Table A3, Table A4, ~~and~~ Table A5 and Table A6 near here)

## 756 **Appendix B: Supporting material for the Results**

757 (Figure B1, Figure B2 and Figure B3 near here)

## 758 **Author Contribution**

759 AB and FS designed the study. AB, NG, HG, CM, JS carried out data processing and delimited fire progressions. BM carried  
760 out FRE data processing. AB assembled the database, performed data analysis and wrote the first version of the manuscript.  
761 All authors contributed to the interpretation of the results and writing of the manuscript.

## 762 **Competing interests**

763 The authors declare that they have no conflict of interest.

## 764 **Acknowledgements**

765 We thank Florian Briquemont for initial data processing and progression delimitation; FEPC personnel ~~that~~ provided relevant  
766 fire to reconstruct some of the wildfires: Pedro Machado, Eduardo Marques, Marco Pires, Marco Lucas, Miguel Martins,  
767 Daniel Santana and Vítor Caramelo. We would also like to thank other fire personnel ~~that-who~~ provided relevant fire data:  
768 João Pedro Costa (AFOCELCA), José Silva (AFOCELCA), António Louro (CM-Mação), Sónia Oliveira (CM-Mação), Rui  
769 Lopes (CBV Peso da Régua), Amélia Freitas (CM Caminha), Rui Pedro Fernandes (CBV Valença), Carlos Gomes (CBV  
770 Boticas), António Ribeiro (ANEPC), Mário Silvestre (ANEPC), Emanuel Oliveira, and Elisio Pereira (CBV Porto de Mós).

771 Finally, we would like to thank ANEPC and FEPC for providing full access to their fire data enabling the development of the  
772 entire work.

773

774 This research was supported by the Forest Research Centre, a research unit funded by Fundação para a Ciência e a Tecnologia  
775 I.P. (FCT), Portugal (UIDB/00239/2020), project foRester (PCIF/SSI/0102/2017) and FIRE-MODSAT II (PTDC/ASP-  
776 SIL/28771/2017) also funded by FCT.

777

778 Akli Benali was funded by FCT through a CEEC contract (CEECIND/03799/2018/CP1563/CT0003). Nuno Guiomar was  
779 funded by the European Union through the European Regional Development Fund in the framework of the Interreg V-A Spain-  
780 Portugal program (POCTEP) under the CILIFO (Ref. 0753\_CILIFO\_5\_E) and FIREPOCTEP (Ref.  
781 0756\_FIREPOCTEP\_6\_E) projects and by National Funds through FCT under the Project UIDB/05183/2020. Paulo  
782 Fernandes contributed in the framework of the FCT-funded project UIDB/04033/2020. Ana Sá was supported under the  
783 framework of the contract-program nr. 1382 (DL 57/2016/CP1382/CT0003).

## 784 **References**

785 Albini, F. A.: Wildland Fires: Predicting the behavior of wildland fires—among nature's most potent forces—can save lives,  
786 money, and natural resources, *Am. Sci.*, 72(6), 590-597, 1984.

787 Alcasena, F., Ager, A., Le Page, Y., Bessa, P., Loureiro, C., and Oliveira, T.: Assessing wildfire exposure to communities and  
788 protected areas in Portugal, *Fire*, 4(4), 82, doi:10.3390/fire404008, 2021.

789 Alexander, M., and Cruz, M. G.: Are the applications of wildland fire behaviour models getting ahead of their evaluation  
790 again?, *Environ. Model. Softw.* (41), 65-71, doi:10.1016/j.envsoft.2012.11.001, 2013.

791 Alexander M. E., and Cruz M. G.: Evaluating a model for predicting active crown fire rate of spread using wildfire  
792 observations, *Can. J. For. Res.*, 36, 3015–3028, doi:10.1139/x06-174, 2006.

793 Alexander, M. E., and Lanoville, R. A.: Wildfires as a source of fire behavior data: a case study from Northwest Territories,  
794 Canada. 9th Conf. Fire and Forest Meteorology, April 21-24, San Diego, CA. American Meteorological Society, Boston, Mass,  
795 86-93, 1987.

796 Alexander, M. E., and Thomas, D. A.: Wildland fire behavior case studies and analyses: Other examples, methods, reporting  
797 standards, and some practical advice, *Fire Manag. Today*, 63(4), 4-12, 2003

798 Andela, N., Morton, D. C., Giglio, L., Paugam, R., Chen, Y., Hantson, S., van der Werf, G. R., and Randerson, J. T.: The  
799 Global Fire Atlas of individual fire size, duration, speed and direction, *Earth Syst. Sci. Data*, 11(2), 529-552, doi:10.5194/essd-  
800 11-529-2019, 2019.

801 Anderson, W. R., Cruz, M. G., Fernandes, P. M., McCaw, L., Vega, J. A., Bradstock, R. A., Fogarty, L. G., Gould, J. B.,  
802 McCarthy, G. H., Marsden-Smedley, J. B., Matthews, S., Mattingley, G., Pearce, H. G., and van Wilgen, B. W.: A generic,

803 empirical-based model for predicting rate of fire spread in shrublands, *Int. J. Wildland Fire*, 24(4), 443-460,  
804 doi:10.1071/WF14130, 2015.

805 Artés, T., Oom, D., De Rigo, D., Durrant, T. H., Maianti, P., Libertà, G., and San-Miguel-Ayanz, J.: A global wildfire dataset  
806 for the analysis of fire regimes and fire behaviour, *Sci. Data*, 6(1), 1-11, doi:10.1038/s41597-019-0312-2, 2019.

807 Benali, A., Guiomar, N., Gonçalves, H., Mota, B., Silva, F., Fernandes, P.M., Mota, C., Penha, A., Santos, J., Pereira, J.M.C.,  
808 and Sá, A.C.L: The Portuguese Large Wildfire Spread Database (PT-FireSprd), <https://doi.org/10.5281/zenodo.7495506> ,  
809 2022.

810 Briones-Herrera, C. I., Vega-Nieva, D. J., Monjarás-Vega, N. A., Briseño-Reyes, J., López-Serrano, P .M., Corral-Rivas, J. J.,  
811 Alvarado-Celestino, E., Arellano-Pérez, S., Álvarez-González, J.G., Ruiz-González, A. D., Jolly, W. M., and Parks, S. A.:  
812 Near real-time automated early mapping of the perimeter of large forest fires from the aggregation of VIIRS and MODIS  
813 active fires in Mexico, *Remote Sens.*, 12(12), 2061, doi:10.3390/rs12122061, 2020.

814 Butler, B. W., and Reynolds, T. D.: Wildfire case study: Butte City, southeastern Utah, July 1, 1994, USDA For. Serv., Intermt.  
815 Res. Stn., Ogden, UT. Gen. Tech. Rep. INT-GTR-351, doi:10.2737/INT-GTR-351, 1997.

816 Catchpole, W. R., Catchpole, E. A., Butler, B. W., Rothermel, R. C., Morris, G. A., and Latham, D. J.: Rate of spread of free-  
817 burning fires in woody fuels in a wind tunnel, *Combust. Sci. Technol.*, 131(1-6), 1-37, doi:10.1080/00102209808935753,  
818 1998.

819 Chen, Y., Hantson, S., Andela, N., Coffield, S. R., Graff, C. A., Morton, D. C., Ott, L.E., Foufoula-Georgiou, E., Smyth, P.,  
820 Goulden, M .L., and Randerson, J. T.: California wildfire spread derived using VIIRS satellite observations and an object-  
821 based tracking system, *Sci. Data*, 9(1), 1-15, doi:10.1038/s41597-022-01343-0, 2022.

822 Cheney, N. P., Gould, J. S., McCaw, W .L., and Anderson, W. R.: Predicting fire behaviour in dry eucalypt forest in southern  
823 Australia., *For. Ecol. Manag.*, 280, 120-131, doi:10.1016/j.foreco.2012.06.012, 2012.

824 Cheney, N. P.: Fire behaviour during the Pickering Brook wildfire, January 2005 (Perth Hills Fires 71-80), *Conserv. Sci. West.*  
825 *Aust.*, 7, 451–468, 2010.

826 Cheney, N., Gould, J., and Catchpole, W.: The Influence of Fuel, Weather and Fire Shape Variables on Fire-Spread in  
827 Grasslands, *Int. J. Wildland Fire*, 3, 31, doi:10.1071/WF9930031, 1993.

828 Coen, J. L., and Riggan, P. J.: Simulation and thermal imaging of the 2006 Esperanza Wildfire in southern California:  
829 application of a coupled weather–wildland fire model, *Int. J. Wildland Fire*, 23(6), 755-770, doi:10.1071/WF12194, 2014.

830 Collins, B. M., Miller, J. D., Thode, A. E., Kelly, M., van Wagtenonk, J. W., and Stephens, S. L.: Interactions among wildland  
831 fires in a long- established Sierra Nevada natural fire area, *Ecosystems* 12, 114–128, doi:10.1007/s10021-008-9211-7, 2019.

832 Countryman, C. M.: The fire environment concept, USDA Forest Service, Pacific Southwest Range and Experiment Station,  
833 Berkeley, California, USA, 1972.

834 Crowley, M. A., Cardille, J. A., White, J. C., and Wulder, M. A.: Generating intra-year metrics of wildfire progression using  
835 multiple open-access satellite data streams, *Remote Sens. Environ.*, 232, 111295, doi:10.1016/j.rse.2019.111295, 2019.

836 Cruz, M. G., Alexander, M. E., and Kilinc, M.: Wildfire rates of spread in grasslands under critical burning conditions, *Fire*,  
837 5(2), 55, doi:10.3390/fire5020055, 2022.

838 Cruz, M. G., Cheney, N. P., Gould, J. S., McCaw, W. L., Kilinc, M., and Sullivan, A. L.: An empirical-based model for  
839 predicting the forward spread rate of wildfires in eucalypt forests, *Int. J. Wildland Fire*, 31(1), 81-95, doi:10.1071/WF21068,  
840 2021.

841 Cruz, M. G., and Alexander, M. E.: The 10% wind speed rule of thumb for estimating a wildfire's forward rate of spread in  
842 forests and shrublands, *Ann. For. Sci.*, 76(2), 1-11, doi:10.1007/s13595-019-0829-8,2019.

843 Cruz, M. G., Alexander, M. E., Sullivan, A. L., Gould, J. S., and Kilinc, M.: Assessing improvements in models used to  
844 operationally predict wildland fire rate of spread, *Environ. Model. Softw.*, 105, 54-63, doi:10.1016/j.envsoft.2018.03.027,  
845 2018.

846 Cruz, M. G., Gould, J. S., Alexander, M. E., Sullivan, A. L., McCaw, W. L., and Matthews, S.: Empirical-based models for  
847 predicting head-fire rate of spread in Australian fuel types, *Aust. For.*, 78(3), 118-158, doi:10.1080/00049158.2015.1055063,  
848 2015.

849 Cruz, M. G., McCaw, W. L., Anderson, W. R., and Gould, J. S.: Fire behaviour modelling in semi-arid mallee-heath shrublands  
850 of southern Australia, *Environ. Model. Softw.*, 40, 21-34, doi:10.1016/j.envsoft.2012.07.003, 2013.

851 Cruz, M. G., and Alexander, M. E.: Uncertainty associated with model predictions of surface and crown fire rates of spread,  
852 *Environ. Model. Softw.*, 47, 16-28, doi:10.1016/j.envsoft.2013.04.004, 2013.

853 Cruz, M. G.: Monte Carlo-based ensemble method for prediction of grassland fire spread, *Int. J. Wildland Fire*, 19(4), 521-  
854 530, doi:10.1071/WF08195, 2010.

855 Cruz, M. G., Alexander, M.E., and Wakimoto, R.H.: Development and testing of models for predicting crown fire rate of  
856 spread in conifer forest stands, *Can. J. For. Res.*, 35(7), 1626-1639, doi:10.1139/x05-085, 2005.

857 Dale, M. R. T., and Fortin, M. J.: From graphs to spatial graphs, *Annu. Rev. Ecol. Evol. Syst.*, 21-38, doi:10.1146/annurev-  
858 ecolsys-102209-144718, 2010.

859 Duff, T. J., Chong, D. M., and Tolhurst, K. G.: Quantifying spatio-temporal differences between fire shapes: Estimating fire  
860 travel paths for the improvement of dynamic spread models, *Environ. Model. Softw.*, 46, 33-43,  
861 doi:10.1016/j.envsoft.2013.02.005, 2013.

862 Fernandes, P. M., Sil, A., Ascoli, D., Cruz, M. G., Rossa, C. G., and Alexander, M. E.: Characterizing fire behavior across the  
863 globe. In: Hood, S. M., Drury, S., Steelman, T., Steffens, R.[eds.]: *Proceedings of the Fire Continuum-Preparing for the future*  
864 *of wildland fire; 2018 May 21-24; Missoula, MT. Proceedings RMRS-P-78. Fort Collins, CO: US Department of Agriculture,*  
865 *Forest Service, Rocky Mountain Research Station. p. 258-263., 78, 258-263, 2020.*

866 Fernandes, P. M., Sil, A., Ascoli, D., Cruz, M. G., Alexander, M. E., Rossa, C. G., Baeza, J., Burrows, N., Davies, G. M.,  
867 Fidelis, A., Gould, J. S., Govender, N., Kilinc, M., and McCaw, L.: Drivers of wildland fire behaviour variation across the  
868 Earth. In: Viegas, D.X. (Ed.), *Advances in Forest Fire Research, Chapter 7 – Short contributions*, 1267-1270,  
869 doi:10.14195/978-989-26-16-506\_154, 2018.

870 Fernandes, P. M., Barros, A. M., Pinto, A., and Santos, J. A.: Characteristics and controls of extremely large wildfires in the  
871 western Mediterranean Basin, *J. Geophys. Res. Biogeosci.*, 121(8), 2141-2157, doi:10.1002/2016JG003389, 2016.

872 Fernandes, P. M., Botelho, H.S., Rego, F.C., and Loureiro, C.: Empirical modelling of surface fire behaviour in maritime pine  
873 stands, *Int. J. Wildland Fire*, 18(6), 698-710, doi:10.1071/WF08023, 2009.

874 Finney, M. A., McAllister, S. S., Forthofer, J. M., and Grumstrup, T. P.: *Wildland Fire Behaviour: Dynamics, Principles and*  
875 *Processes*, CSIRO Pub., 2021.

876 Forestry Canada Fire Danger Group: Development and structure of the Canadian Forest Fire Behavior Prediction System. For.  
877 Can., Ottawa, Ont. Inf. Rep. ST-X-3, 1992.

878 Frantz, D., Stellmes, M., Röder, A., and Hill, J.: Fire spread from MODIS burned area data: Obtaining fire dynamics  
879 information for every single fire, *Int. J. Wildland Fire*, 25(12), 1228-1237, doi:10.1071/WF16003, 2016.

880 Giglio, L., Descloitres, J., Justice, C. O., and Kaufman, Y. J.: An enhanced contextual fire detection algorithm for MODIS,  
881 *Remote Sens. Environ.* 87, 273–282, doi:10.1016/S0034-4257(03)00184-6, 2003

882 Giglio, L., Schroeder, W. and Justice, C. O.: The collection 6 MODIS active fire detection algorithm and fire products. *Remote*  
883 *Sens. Environ.*, 178, pp.31-41, doi:10.1016/j.rse.2016.02.054, 2016.

884 Gollner, M., Trouve, A., Altintas, I., Block, J., de Callafon, R., Clements, C., Cortes, A., Ellicott, E., Filippi, J. B., Finney, M.,  
885 Ide, K., Jenkins, M.A., Jimenez, D., Lautenberger, C., Mandel, J., Rochoux, M., and Simeoni, A.: Towards data-driven  
886 operational wildfire spread modeling: A report of the NSF-funded WIFIRE workshop, 2015.

887 Guerreiro, J., Fonseca, C., Salgueiro, A., Fernandes, P., Iglésias, E. L., Neufville, R., Mateus, P., Castellnou, M., Silva, J. S.,  
888 Moura, J. M., Rego, F. C., and Caldeira, D.: Análise e apuramento dos factos relativos aos incêndios que ocorreram em  
889 Pedrogão Grande, Castanheira de Pêra, Ansião, Alvaiázere, Figueiró dos Vinhos, Arganil, Góis, Penela, Pampilhosa da Serra,  
890 Oleiros e Sertã, entre 17 e 24 de junho de 2017. Comissão Técnica Independente, Assembleia da República, Lisboa.  
891 [https://www.parlamento.pt/Documents/2017/Outubro/RelatórioCTI\\_VF.pdf](https://www.parlamento.pt/Documents/2017/Outubro/RelatórioCTI_VF.pdf), 2017.

892 Guerreiro, J., Fonseca, C., Salgueiro, A., Fernandes, P., Iglésias, E. L., Neufville, R., Mateus, P., Castellnou, M., Silva, J. S.,  
893 Moura, J. M., Rego, F. C., and Caldeira, D.: Avaliação dos Incêndios ocorridos entre 14 e 16 de outubro de 2017 em Portugal  
894 Continental. Comissão Técnica Independente, Assembleia da República, Lisboa.  
895 <https://www.parlamento.pt/Documents/2018/Marco/RelatorioCTI190318N.pdf>, 2018.

896 Humber, M., Zubkova, M., and Giglio, L.: A remote sensing-based approach to estimating the fire spread rate parameter for  
897 individual burn patch extraction, *Int. J. Remote Sens.*, 43(2), 649-673, doi:10.1080/01431161.2022.2027544, 2022.

898 Hirsch, K. G., and Martell, D. L. A review of initial attack fire crew productivity and effectiveness, *Int. J. Wildland Fire*, 6(4),  
899 199-215, doi:10.1071/WF9960199, 1996.

900 Khanmohammadi, S., Arashpour, M., Golafshani, E. M., Cruz, M. G., Rajabifard, A., and Bai, Y.: Prediction of wildfire rate  
901 of spread in grasslands using machine learning methods, *Environ. Model. Softw.*, 156, 105507,  
902 doi:10.1016/j.envsoft.2022.105507, 2022.

903 Kilinc, M., Anderson, W., and Price, B.: The Applicability of Bushfire Behaviour Models in Australia. Victorian Government,  
904 Department of Sustainability and Environment. DSE Schedule 5: Fire Severity Rating Project, Melbourne, VIC. Technical  
905 Report 1, 2012.

906 McCaw, W. L., Gould, J. S., Cheney, N. P., Ellis, P. F. M., and Anderson, W. R.: Changes in behaviour of fire in dry eucalypt  
907 forest as fuel increases with age, *For. Ecol. Manag.* 271, 170-181, doi:10.1016/j.foreco.2012.02.003, 2012.

908 [Niro, F., Goryl, P., Dransfeld, S., Boccia, V., Gascon, F., Adams, J., Themann, B., Scifoni, S. and Doxani, G.: European Space](#)  
909 [Agency \(ESA\) Calibration/Validation Strategy for Optical Land-Imaging Satellites and Pathway towards Interoperability,](#)  
910 [Remote Sens., 13, 3003, doi:10.3390/rs13153003, 2021.](#)

911 Oom, D., Silva, P. C., Bistinas, I., and Pereira, J. M. C.: Highlighting biome-specific sensitivity of fire size distributions to  
912 time-gap parameter using a new algorithm for fire event individuation, *Remote Sens.*, 8(8), 663, doi:10.3390/rs8080663, 2016.

913 Palaiologou, P., Kalabokidis, K., Ager, A. A., and Day, M. A.: Development of Comprehensive Fuel Management Strategies  
914 for Reducing Wildfire Risk in Greece, *Forests*, 11(8), 789, doi:10.3390/f11080789, 2020.

915 Palheiro, P. M., Fernandes, P. M., Cruz, M. G.: A fire behaviour-based fire danger classification for maritime pine stands:  
916 comparison of two approaches, *For. Ecol. Manag.*, (234), S54, doi:10.1016/j.foreco.2006.08.075, 2006.

917 Parisien M. A., Parks S. A., Miller C., Krawchuk M. A., Heathcott M., and Moritz M. A.: Contributions of ignitions, fuels,  
918 and weather to the burn probability of a boreal landscape, *Ecosystems* 14, 1141–1155, doi:10.1007/s10021-011-9474-2, 2011.

919 Parks, S. A.: Mapping day-of-burning with coarse-resolution satellite fire-detection data, *Int. J. Wildland Fire*, 23(2), 215-223,  
920 doi:10.1071/WF13138, 2014.

921 Pereira, M. G., Malamud, B. D., Trigo, R. M., and Alves, P.I.: The history and characteristics of the 1980–2005 Portuguese  
922 rural fire database, *Nat. Hazards Earth Syst. Sci.*, 11(12), 3343-3358, doi:10.5194/nhess-11-3343-2011, 2011.

923 [Pereira, J. M., Oom, D., Silva, P. C., and Benali, A.: Wild, tamed, and domesticated: Three fire macroregimes for global](#)  
924 [pyrogeography in the Anthropocene, Ecol. Appl., 32\(6\), e2588, doi:10.1002/eap.2588, 2022.](#)

925 [Pinto, M. M., DaCamara, C. C., Trigo, I. F., Trigo, R. M., and Turkman, K. F.: Fire danger rating over Mediterranean Europe](#)  
926 [based on fire radiative power derived from Meteosat, Nat. Hazards Earth Syst. Sci., 18\(2\), 515-529, doi:10.5194/nhess-2017-](#)  
927 [346, 2018.](#)

928 Rodríguez y Silva, F., and Molina-Martínez, J.R.: Modeling Mediterranean forest fuels by integrating field data and mapping  
929 tools, *Eur. J. For. Res.*, 131, 571–582, doi:10.1007/s10342-011-0532-2, 2012.

930 Rothermel, R.C.: A mathematical model for predicting fire spread in wildland fuels, Res. Pap. INT-115. Ogden, UT: U.S.  
931 Department of Agriculture, Intermountain Forest and Range Experiment Station, 1972.

932 Sá, A. C., Benali, A., Fernandes, P. M., Pinto, R. M., Trigo, R. M., Salis, M., Russo, A., Jerez, S., Soares, P. M. M., Schroeder,  
933 W., and Pereira, J. M. C.: Evaluating fire growth simulations using satellite active fire data, *Remote Sens. Environ.*, 190, 302-  
934 317, doi:10.1016/j.rse.2016.12.023, 2017.

935 Salis, M., Del Giudice, L., Arca, B., Ager, A. A., Alcasena-Urdiroz, F., Lozano, O., Bacciu, V., Spano, D., and Duce, P.:  
936 Modeling the effects of different fuel treatment mosaics on wildfire spread and behavior in a Mediterranean agro-pastoral area.  
937 *J. Environ. Manage.*, 212, 490-505, doi:10.1016/j.jenvman.2018.02.020, 2018.

938 Santoni, P.-A., J.-B. Filippi, J.-H. Balbi, and Bosseur, F.: Wildland fire behaviour case studies and fuel models for landscape-  
939 scale fire modeling, *J. Combust.*, 613424, doi:10.1155/2011/613424, 2011.

940 Schag, G. M., Stow, D. A., Riggan, P. J., Tissell, R. G., and Coen, J. L.: Examining landscape-scale fuel and terrain controls  
941 of wildfire spread rates using repetitive airborne thermal infrared (ATIR) imagery, *Fire*, 4(1), 6, doi:10.3390/fire4010006,  
942 2021.

943 Schroeder, W., Oliva, P., Giglio, L., and Csizsar, I. A.: The New VIIRS 375 m active fire detection data product: Algorithm  
944 description and initial assessment, *Remote Sens. Environ.*, 143, 85-96, doi:10.1016/j.rse.2013.12.008, 2014.

945 Schroeder, W.: Visible Infrared Imaging Radiometer Suite (VIIRS) 375 m & 750 m Active Fire Detection Data Sets Based on  
946 NASA VIIRS Land Science Investigator Processing System (SIPS) Reprocessed Data—Version 1. 2017.

947 Scott, J. H., and Reinhardt, E. D.: Assessing Crown Fire Potential by Linking Models of Surface and Crown Fire Behavior,  
948 US Department of Agriculture, Forest Service, Rocky Mountain Research Station, Fort Collins, CO. Research Paper RMRS-  
949 RP-29, doi:10.2737/RMRS-RP-29, 2001.

950 Sharples, J. J., McRae, R. H., and Wilkes, S. R.: Wind–terrain effects on the propagation of wildfires in rugged terrain: fire  
951 channelling, *Int. J. Wildland Fire*, 21(3), 282-296, doi:10.1071/WF10055, 2012.

952 Sifakis, N. I., Iossifidis, C., Kontoes, C., and Keramitsoglou, I.: Wildfire detection and tracking over Greece using  
953 MSG-SEVIRI satellite data, *Remote Sens.*, 3(3), 524-538, doi:10.3390/rs3030524, 2011.

954 Stocks, B. J., Alexander, M. E., Wotton, B. M., Stefner, C. N., Flannigan, M. D., Taylor, S. W., Lavoie, N., Mason, J. A.,  
955 Hartley, G. R., Maffey, M. E., Dalrymple, G. N., Blake, T. W., and Cruz, M. G., Lanoville, R. A.: Crown fire behaviour in a  
956 northern jack pine black spruce forest, *Can. J. For. Res.* 34, 1548-1560, doi:10.1139/x04-054, 2004.

957 Storey, M. A., Price, O. F., Sharples, J. J., and Bradstock, R. A.: Drivers of long-distance spotting during wildfires in south-  
958 eastern Australia, *Int. J. Wildland Fire*, 29(6), 459-472, doi:10.1071/WF19124, 2020.

959 Storey, M. A., Bedward, M., Price, O. F., Bradstock, R. A., and Sharples, J. J.: Derivation of a Bayesian fire spread model  
960 using large-scale wildfire observations, *Environ. Model. Softw.*, 144, 105127, doi:10.1016/j.envsoft.2021.105127, 2021.

961 [Stow, D.A., Riggan, P.J., Storey, E.A., and Coulter, L.L.: Measuring fire spread rates from repeat pass airborne thermal infrared](#)  
962 [imagery. Remote Sens. Lett., 5, 803–812, doi:10.1080/2150704X.2014.967882, 2014.](#)

963 Vaillant, N. M., Ewell, C.M., and Fites-Kaufman, J. A.: Capturing crown fire behavior on wildland fires - the Fire Behavior  
964 Assessment Team in action, *Fire Manag. Today* 73(4):41-45, 2014.

965 Valero, M. M., Rios, O., Pastor, E., and Planas, E.: Automated location of active fire perimeters in aerial infrared imaging  
966 using unsupervised edge detectors, *Int. J. Wildland Fire*, 27(4), 241-256, doi:10.1071/WF17093, 2018.

967 Veraverbeke, S., Sedano, F., Hook, S. J., Randerson, J. T., Jin, Y., and Rogers, B. M.: Mapping the daily progression of large  
968 wildland fires using MODIS active fire data, *Int. J. Wildland Fire*, 23(5), 655-667, doi:10.1071/WF13015, 2014.

969 Viegas, D. X., Almeida, M. F., Ribeiro, L. M., Raposo, J., Viegas, M. T., Oliveira, R., Alves, D., Pinto, C., Rodrigues, A.,  
970 Ribeiro, C., Lopes, S., Jorge, H., and Viegas, C. X.: Análise dos Incêndios Florestais Ocorridos a 15 de outubro de 2017,  
971 Centro de Estudos sobre Incêndios Florestais (CEIF/ADAI/LAETA), 2019.

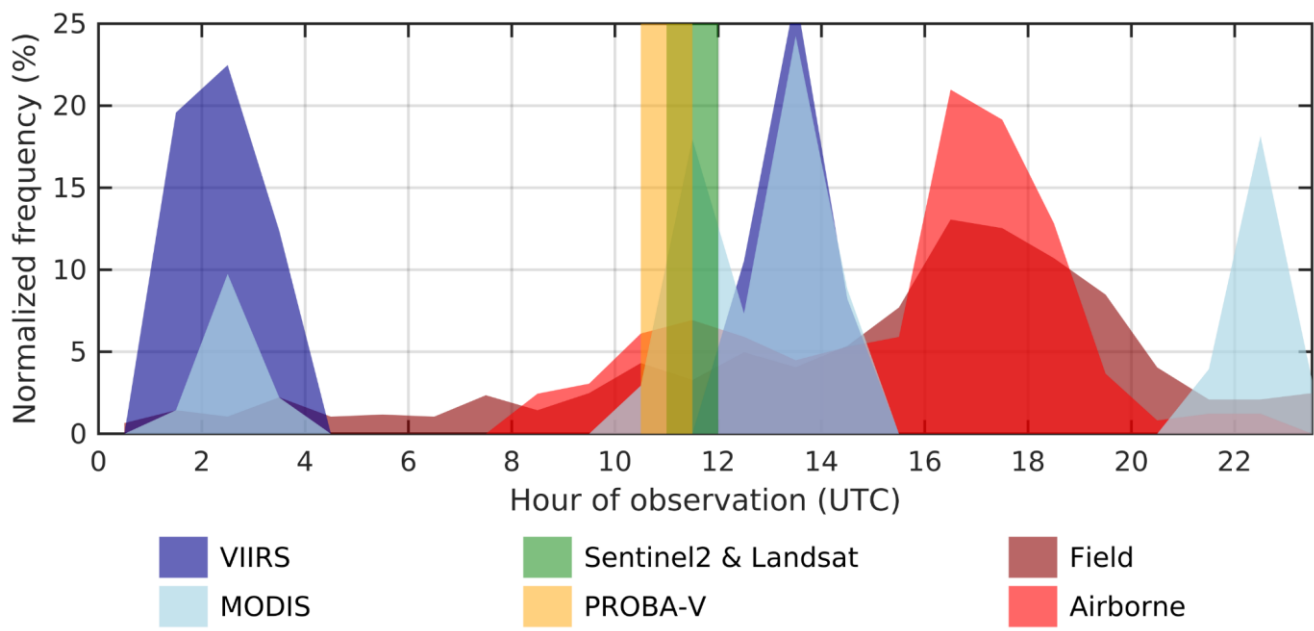
972 Wade, D. D., and Ward, D. E.: An analysis of the Air Force Bomb Range Fire. Res. Pap. SE-105. Asheville, NC, USDA  
973 Forest Service, Southeastern Forest Experiment Station, 1973.

974 Wolfe, R. E., Roy, D. P., and Vermote, E.: MODIS land data storage, gridding, and compositing methodology: level 2 grid,  
975 IEEE Trans. Geosci. Remote Sens. 36, doi:10.1109/36.701082, 1998.

976 Wooster, M. J., Roberts, G., Freeborn, P. H., Xu, W., Govaerts, Y., Beeby, R., He, J., Lattanzio, A., Fisher, D., and Mullen,  
977 R.: LSA SAF Meteosat FRP products – Part 1: Algorithms, product contents, and analysis, Atmos. Chem. Phys., 15, 13217–  
978 13239, doi:10.5194/acp-15-13217-2015, 2015.

979 Wotton, B. M.: Interpreting and using outputs from the Canadian Forest Fire Danger Rating System in research applications,  
980 Environ. Ecol. Stat., 16(2), 107-131, doi:10.1007/s10651-007-0084-2, 2009.

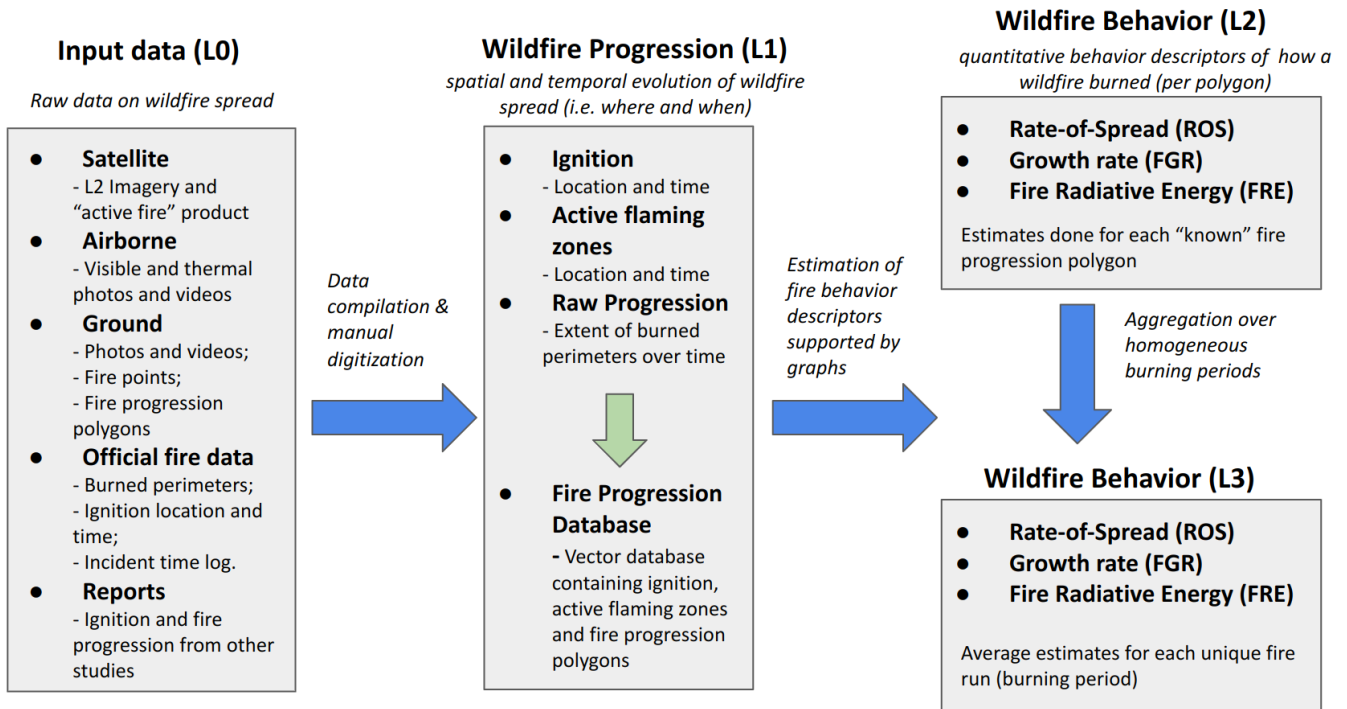
981  
982  
983



985  
986

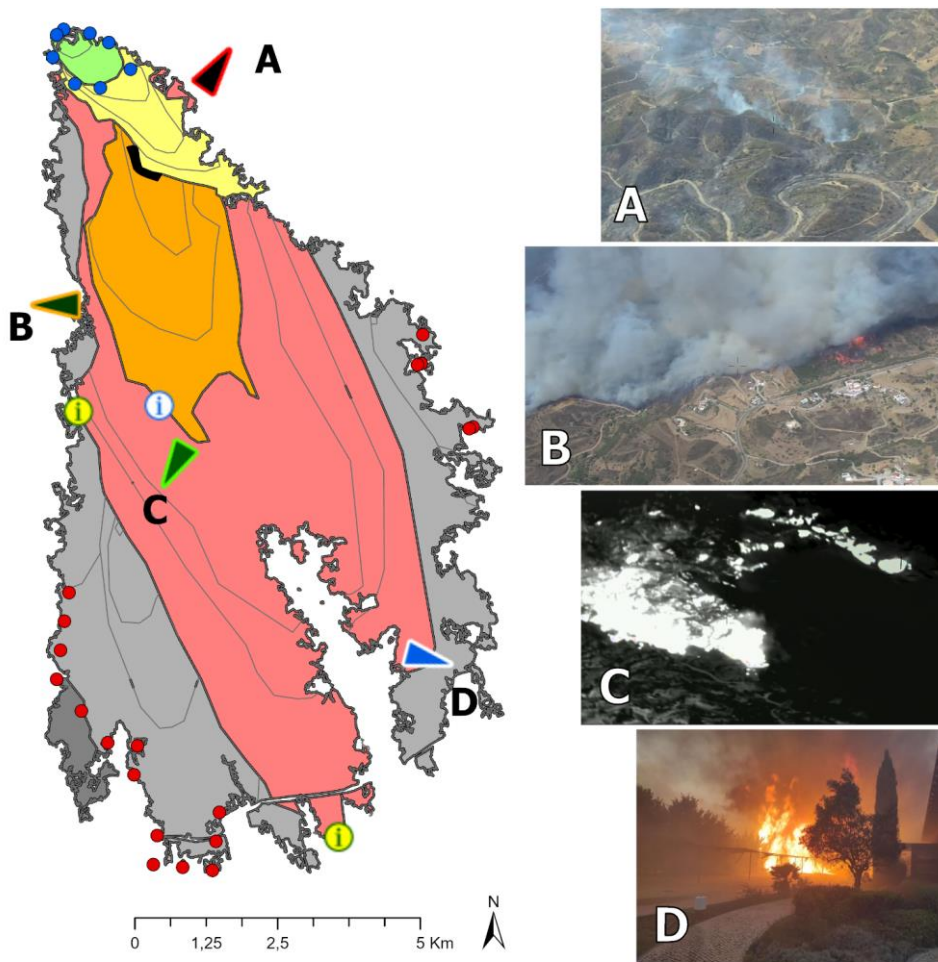
987 **Figure 1: Hourly frequency of observations in active wildfires acquisitions for satellite, field and airborne data. The data used refers to the year 2019 as an example. The frequency is normalised by dividing the number of observations by the total of each data source.**  
 988 **Sentinel-2, Landsat and PROBA-V refer to the temporal windows and not the frequency, since all of the data are acquired in a very short window. The time windows of Sentinel-3 are similar to those of MODIS. MSG-SEVIRI data are not represented since it has a**  
 989 **15' frequency. Acronyms are described in the Data and Methods section.**  
 990  
 991

992



993  
 994  
 995  
 996  
 997

**Figure 2: Flowchart that represents an overview of the data and methods used in the development of the PT-FireSprd database.**



### Input data

#### Satellite data (VIIRS thermal anomalies)

- 2021-08-16 03:09
- 2021-08-17 02:47

#### Airborne and fire operatives data

- ▼ A – Airplane, reactivation (2021-08-16 11:32)
- ▼ B – Airplane, right flank (2021-08-16 16:26)
- ▼ C – Airplane (thermal), fire front (2021-08-16 16:38)
- ▼ D – Operatives, fire front (2021-08-16 19:30)

#### Reports

- ⓘ Location reported in timeline (2021-08-16 16:18)
- ⓘ Locations reported in timeline (2021-08-16 19:30)

### Estimated Fire Progression

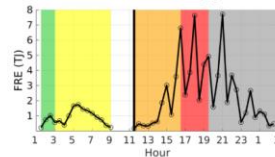
#### Ignition/active flaming zones

- Reactivation Zone (2021-08-16 11:30)

#### Fire perimeters

- 2021-08-16 03:00
- 2021-08-16 09:00
- 2021-08-16 16:30
- 2021-08-16 19:30
- 2021-08-17 03:00
- 2021-08-17 12:00
- Intermediate perimeters

#### Fire Radiative Energy

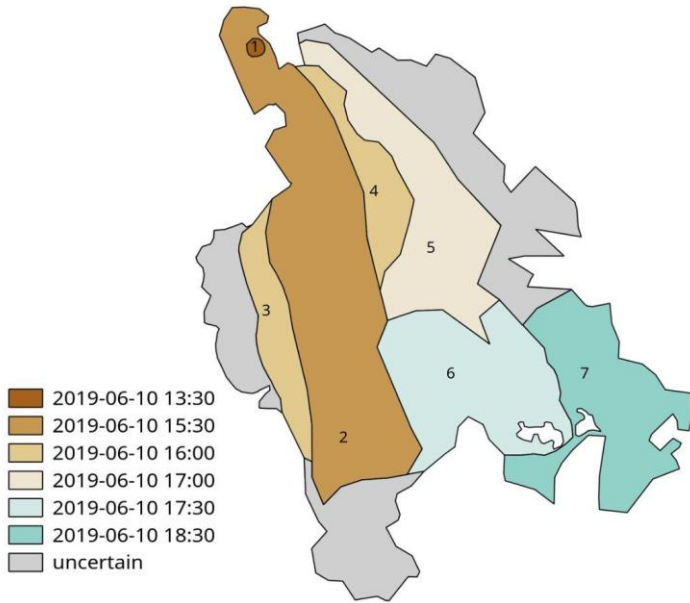


998  
999

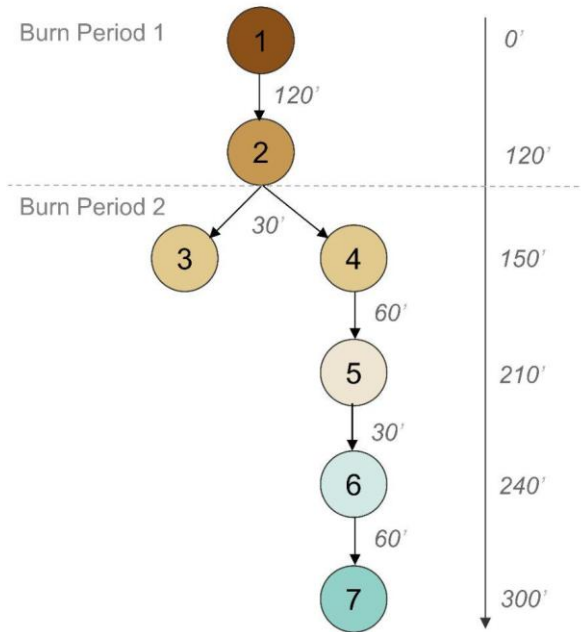
1000  
1001

**Figure 3:** Example of multi-source data integration to derive fire perimeters and reconstruct the progression of the Castro Marim (2021) wildfire. The lines represent different progression polygons. Photos A, B, C, D were kindly provided by ANEPC\FEPC

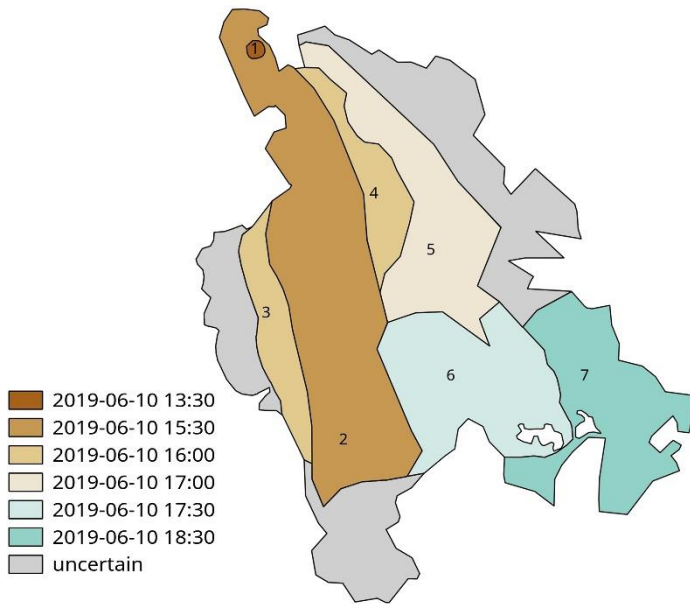
### a) Fire progression



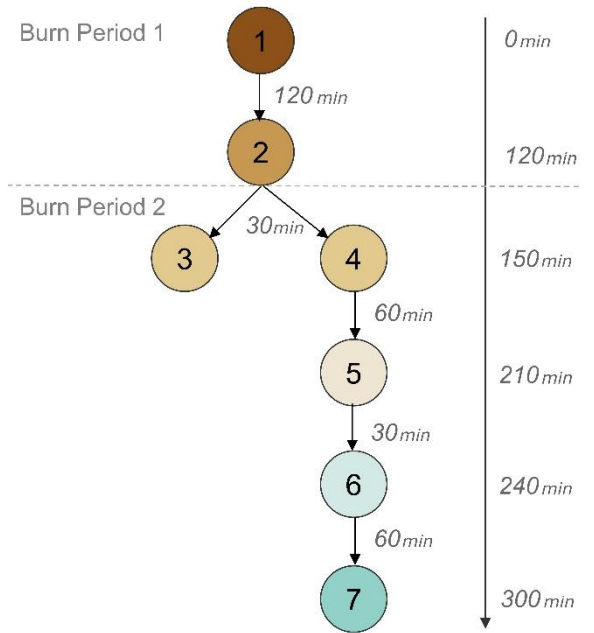
### b) Di-graph structure



### a) Fire progression



### b) Di-graph structure



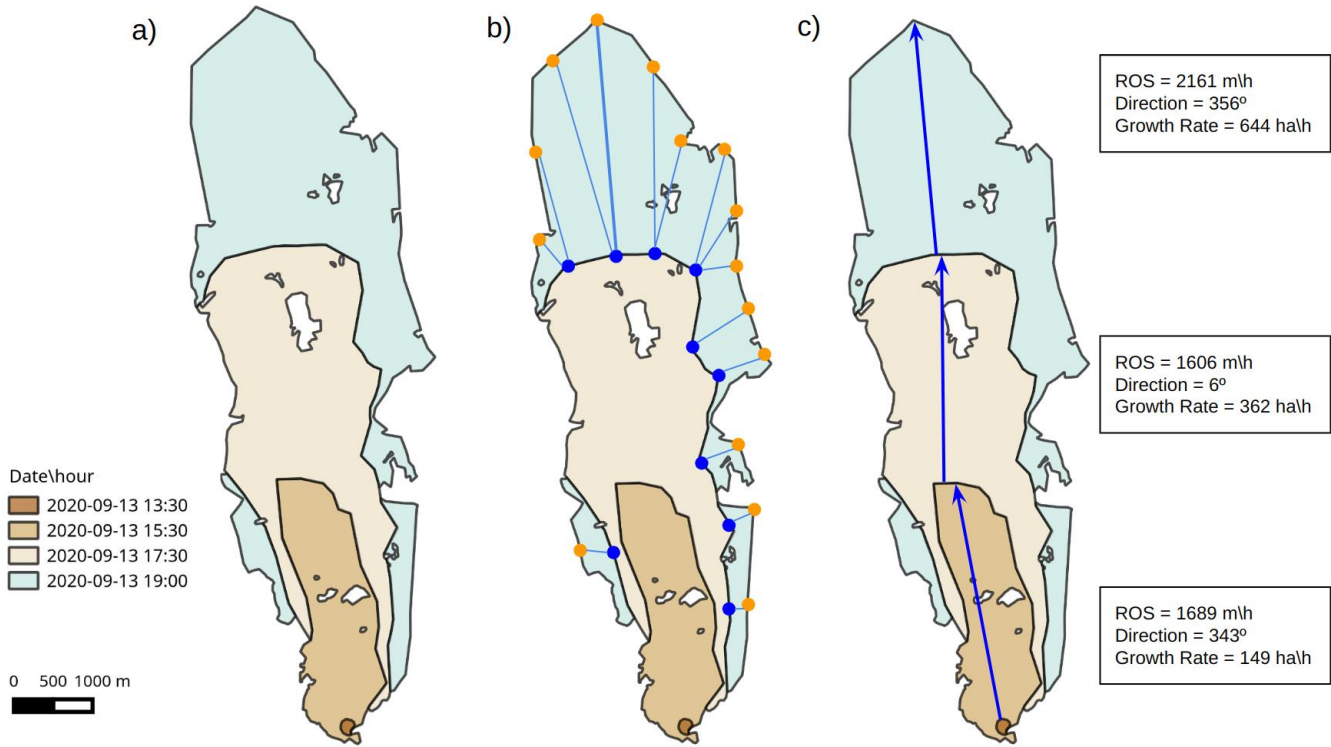
1002

1003

1004

1005  
1006  
1007  
1008

**Figure 4:** Example of how the estimated fire progression (a) of the Ourique 2019 wildfire (a) was used to build the digraph (b). Each node corresponds to a fire progression polygon, identified in (a), and the edges correspond to the time elapsed (in minutes) between each node.



1009  
1010

**Figure 5:** Example of how the fire behaviour descriptors are calculated based on the Proença-a-Nova (2020) wildfire: a) partial fire progression; b) procedure to calculate the distance for each vertex of the pair of consecutive polygons; and c) estimated main spread axis and associated fire behaviour descriptors.

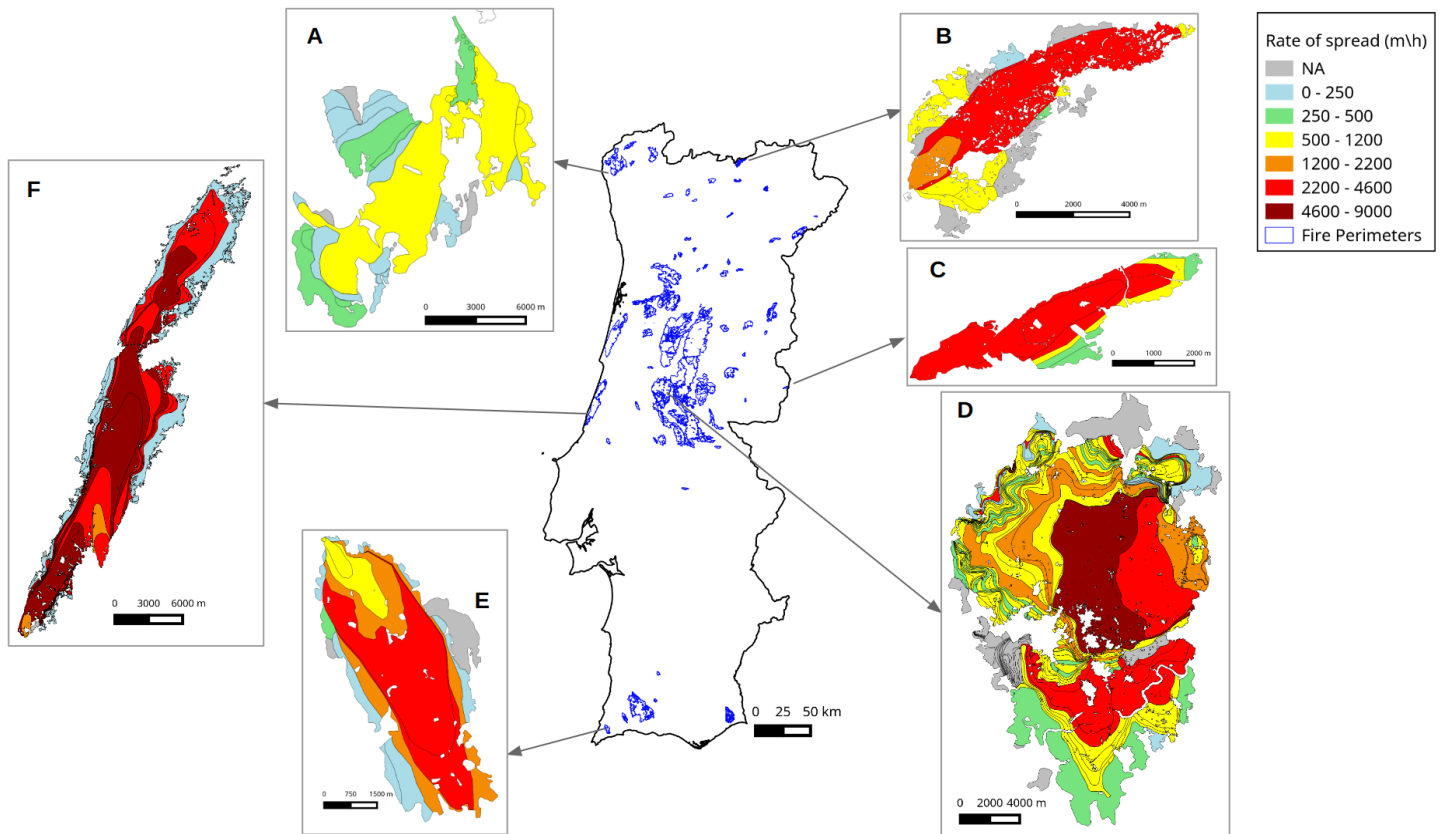


**Figure 6: Overall spatial distribution of the wildfire perimeters in the PT-FireSprd database, with examples of ROS estimates for 6 wildfires: A-Paredes de Coura (2016); B-Chaves (2020); C-Idanha-a-Nova (2020); D-Pedrógão Grande (2017); E-Aljezur (2020); F-Alcobaça (2017).**

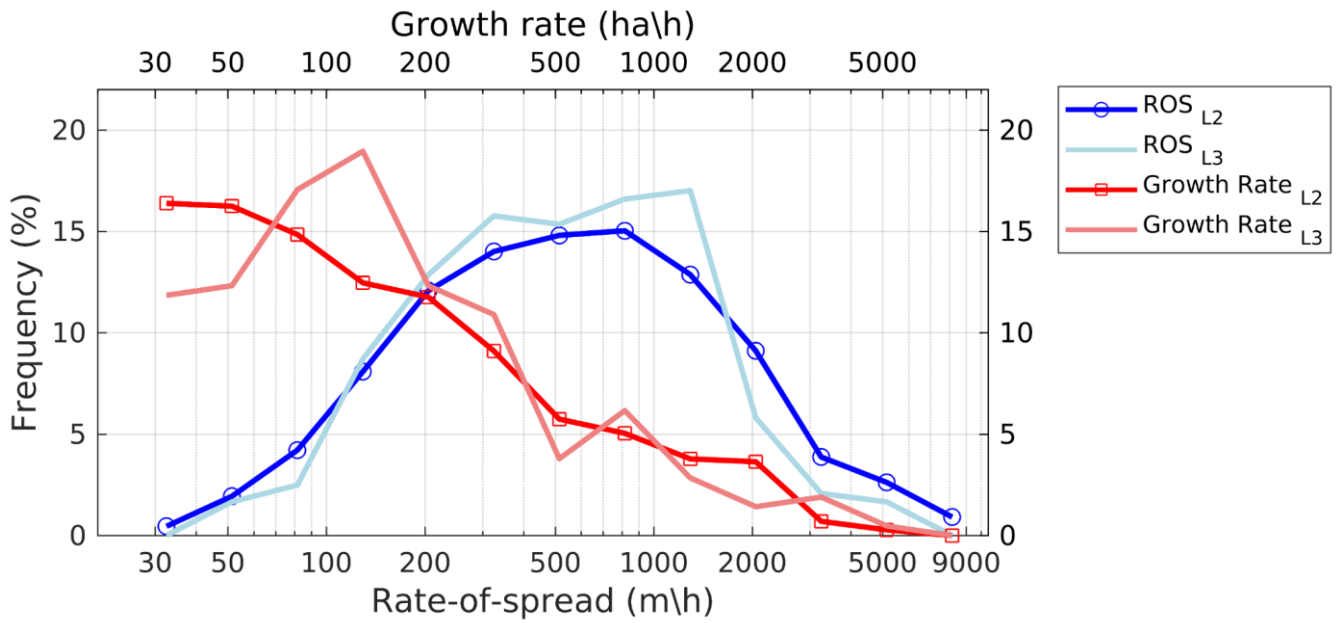
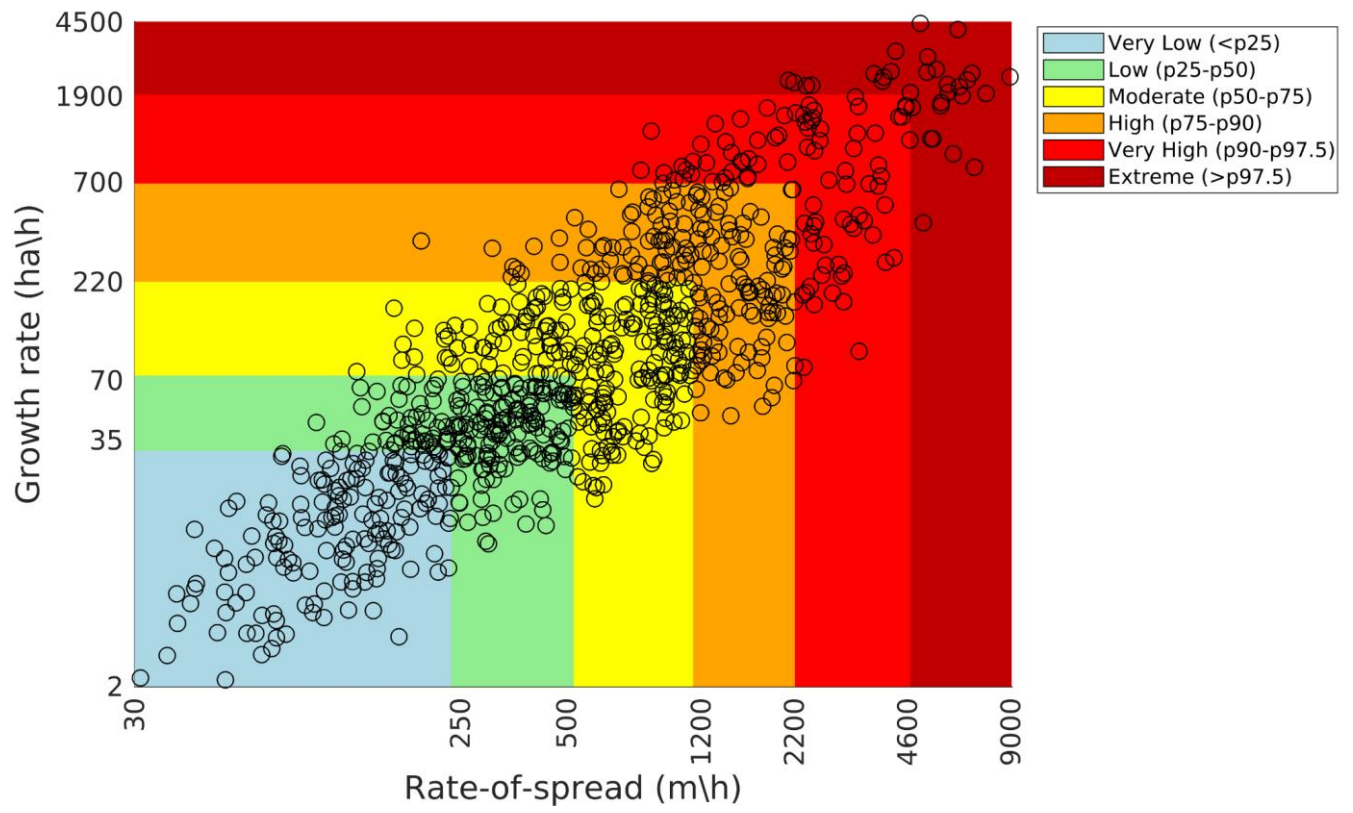


Figure 7: **Histogram of the E-estimated ROS and FGR distributions** for L2 and L3 data (in log-scale). Each point represents the frequency in evenly spaced bins on a logarithmic scale.



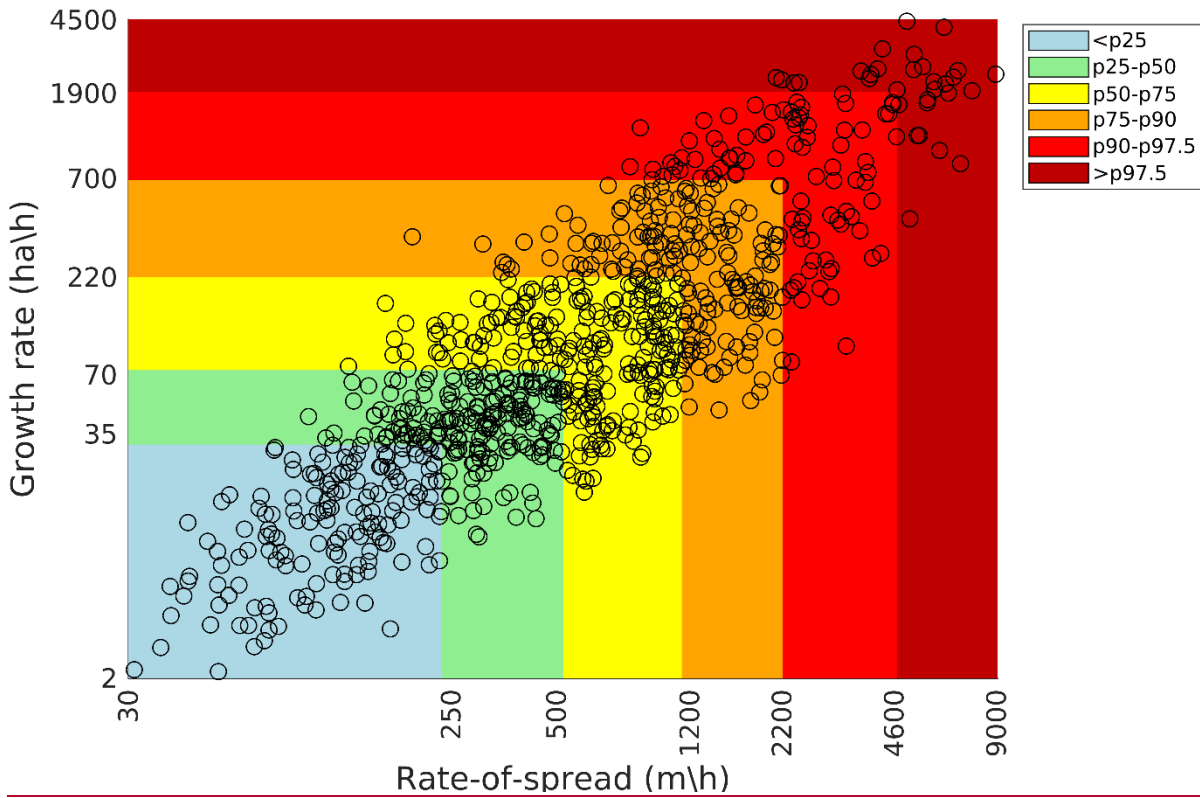
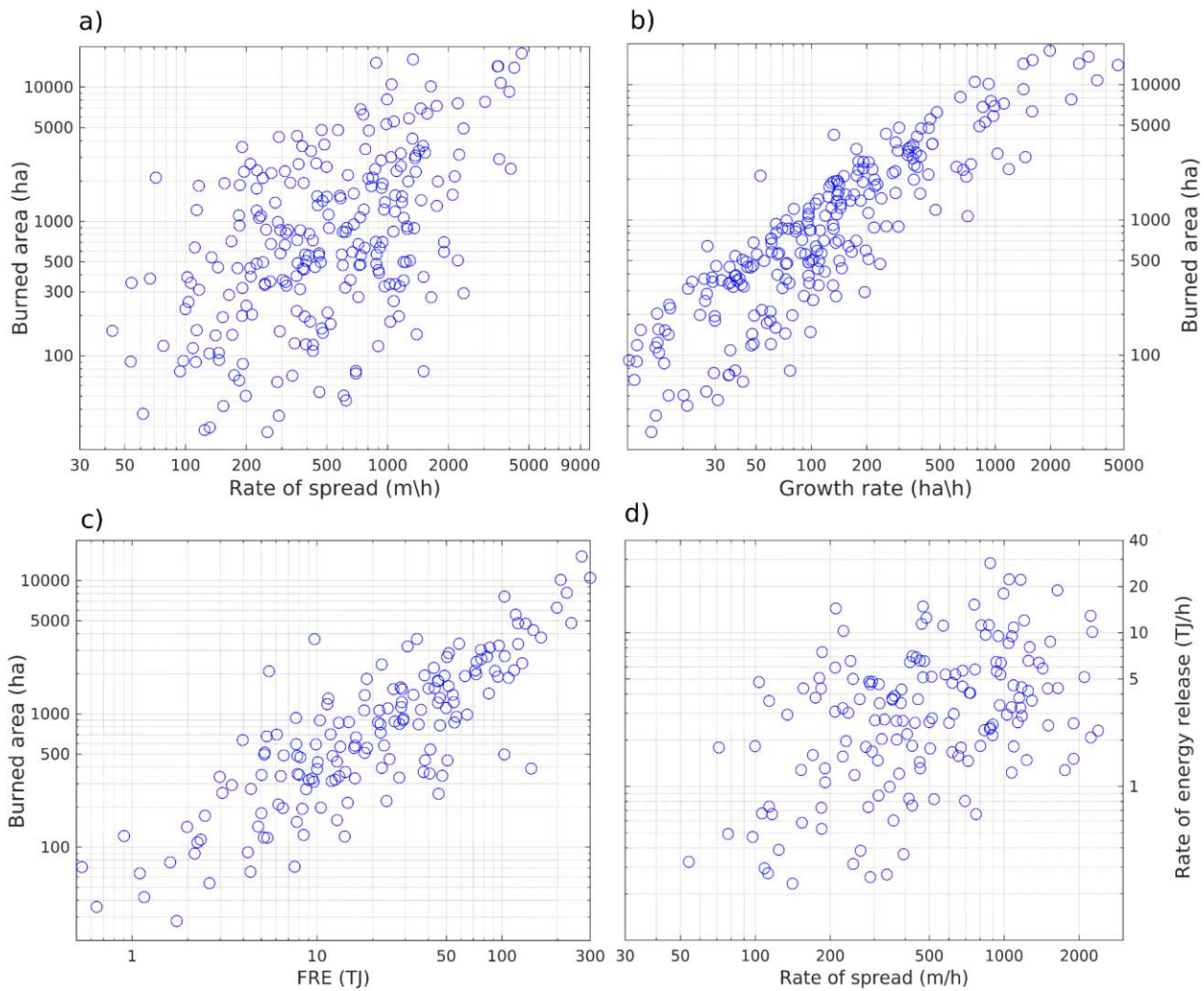
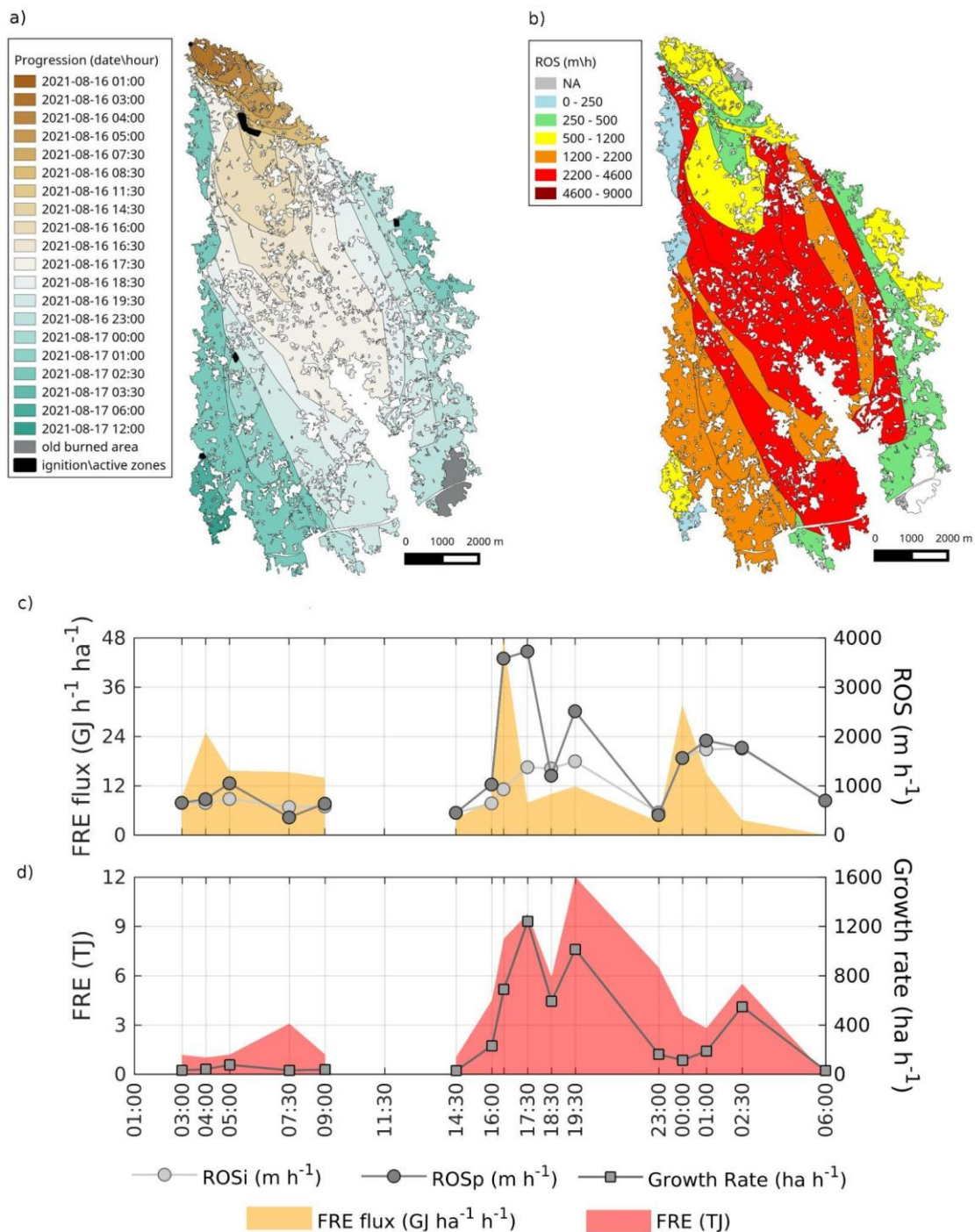


Figure 8: Distribution of the estimated partial rate-of-spread (ROSp) and FGR (L2). Each point represents a wildfire progression with at least 25 ha of extent. The percentiles were calculated for each variable separately (n=874). Colors represent percentile intervals for both fire behaviour descriptors.



**Figure 9: Comparison between simplified wildfire behaviour descriptors (L3): burned area extent and ROS (a), burned area extent and FGR (b), burned area extent and FRE (c), and ROS and average rate of energy release (d). The latter was calculated by dividing the total FRE by the burning period duration.**



**Figure 10: The Castro Marim (2021) wildfire progression (a). Wildfire behaviour descriptors include: the spatial distribution of ROS (b); the temporal distribution of ROS and FRE flux rate (c); and the temporal distribution of FRE and FGR (d). Plots (c) and (d) start at 01:00 of the 16th of August and end at 06:00 of the 17th of August.**

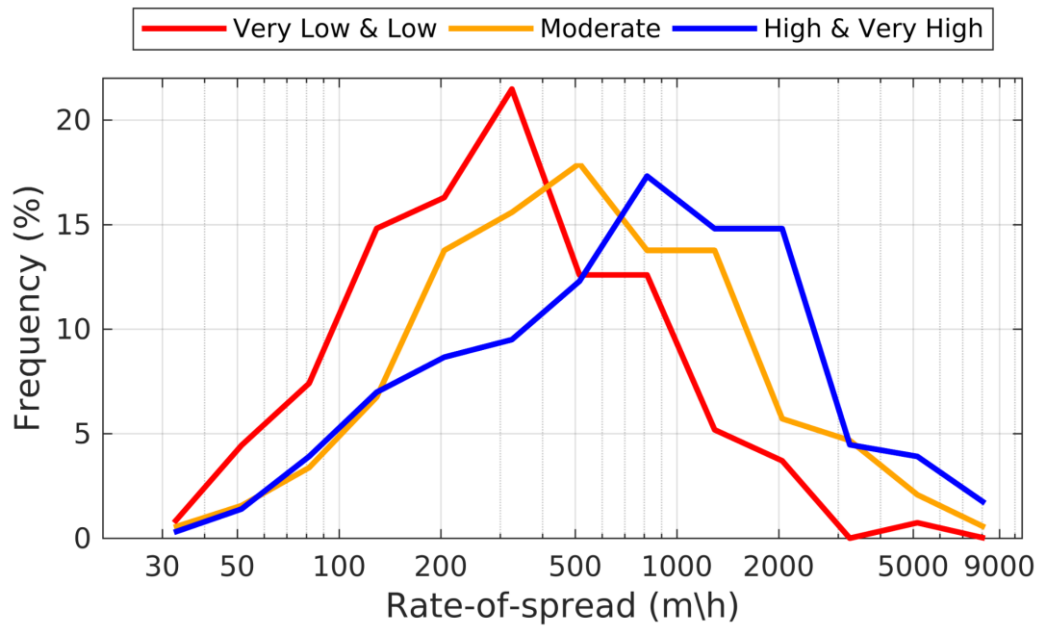


**Figure B1: Histogram of the estimated ROS (L2) for three aggregated levels of confidence. L2 ROS estimates were used and the confidence flags are explained in Table A1.**

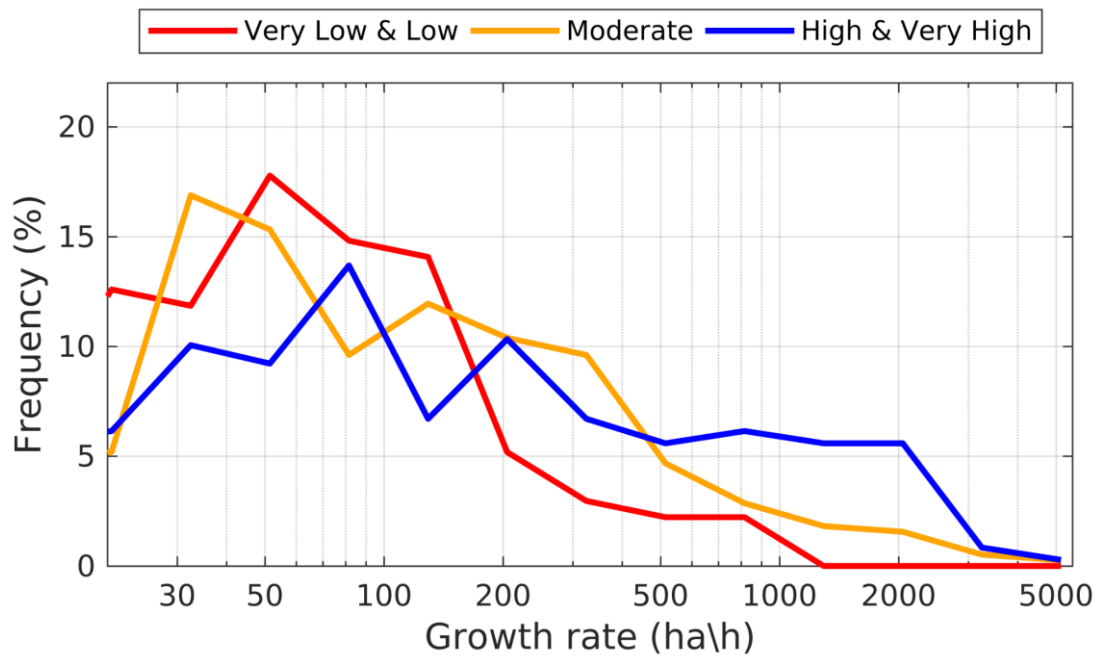


**Figure B2: Histogram of the estimated FGR for three levels of confidence. L2 FGR estimates were used and the confidence flags are explained in Table A1.**

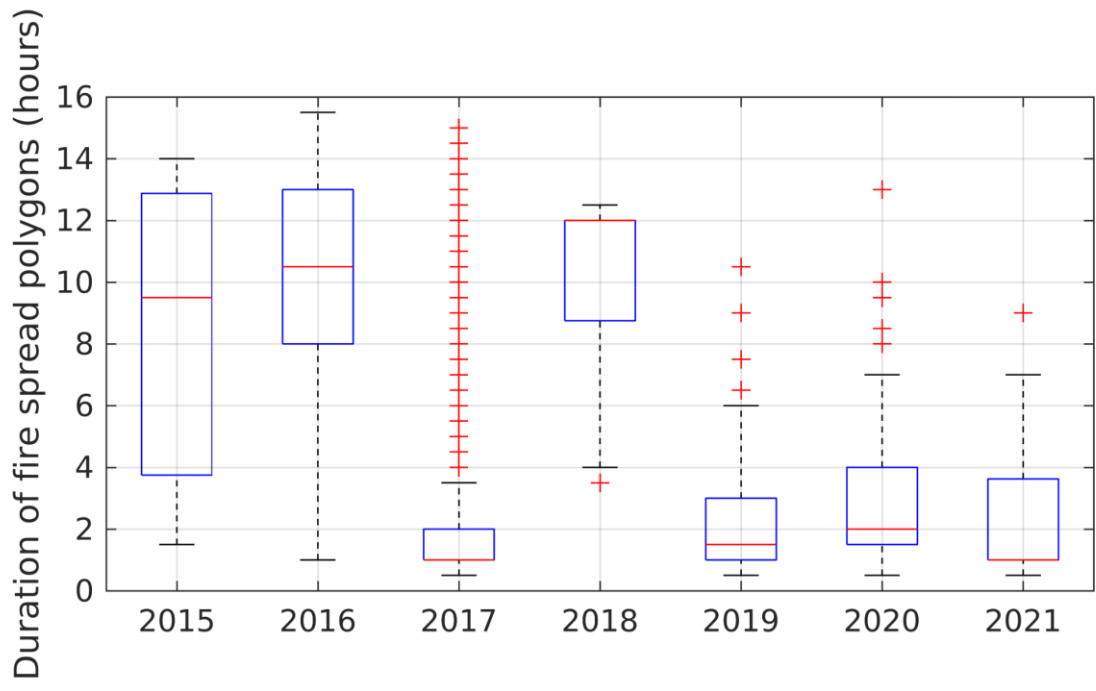


**Figure B3: Distribution of the duration of the progression polygons divided by years**

## Tables

**Table A1. Summary of major data sources and associated characteristics**

<u>Source</u>	<u>Description</u>	<u>Type of data</u>	<u>Temporal frequency</u>	<u>Spatial Resolution</u>
<u>Airborne</u>	<u>Initial-attack heli-brigades</u>	<u>Visible imagery</u>	<u>Depends on fire occurrence; up to the first 30min after wildfire alert</u>	<u>na</u>
<u>Airborne</u>	<u>Aeroplane</u>	<u>Visible, IR and thermal imagery and videos</u>	<u>Depends on fire occurrence; up to four flights per days</u>	<u>&lt;1m*</u>
<u>Airborne</u>	<u>Coordination Helicopter</u>	<u>Visible images</u>	<u>Depends on fire occurrence</u>	<u>na</u>
<u>Satellite</u>	<u>Sentinel-2 (S2)</u>	<u>Visible and IR imagery</u>	<u>Every 5 days</u>	<u>10m – 60m</u>
<u>Satellite</u>	<u>Landsat 8/9</u>	<u>Visible and IR imagery</u>	<u>Every 5 days</u>	<u>30m</u>
<u>Satellite</u>	<u>PROBA V</u>	<u>Visible and IR imagery</u>	<u>Daily** and every 5 days***</u>	<u>**300m; ***100m</u>
<u>Satellite</u>	<u>VIIRS NPP and NOAA-20</u>	<u>Visible and IR imagery</u>	<u>Up to 4 times per day</u>	<u>375m-750m</u>
<u>Satellite</u>	<u>VIIRS NPP and NOAA-20</u>	<u>Thermal anomalies</u>	<u>Up to 4 times per day</u>	<u>375m</u>
<u>Satellite</u>	<u>MODIS Terra and Aqua</u>	<u>Visible and IR imagery</u>	<u>Up to 4 times per day</u>	<u>250m-1000m</u>
<u>Satellite</u>	<u>MODIS Terra and Aqua</u>	<u>Thermal anomalies</u>	<u>Up to 4 times per day</u>	<u>1000m</u>
<u>Satellite</u>	<u>Sentinel 3</u>	<u>Visible and IR imagery</u>	<u>Twice per day (SLSTR), once per day (OLCI)</u>	<u>300-1000m</u>
<u>Satellite</u>	<u>MSG-SEVIRI</u>	<u>Thermal anomalies</u>	<u>Every 15 min</u>	<u>4000 m</u>
<u>Ground</u>	<u>Fire operatives</u>	<u>Visible imagery and videos</u>	<u>Depends on fire occurrence</u>	<u>na</u>
<u>Ground</u>	<u>Fire operatives</u>	<u>Georeferenced points and polygons</u>	<u>Depends on fire occurrence</u>	<u>na</u>
<u>Official fire data</u>	<u>Burned area</u>	<u>Perimeters</u>	<u>annual</u>	<u>na (derived from S2 imagery)</u>
<u>Official fire data</u>	<u>Ignition</u>	<u>Point</u>	<u>annual</u>	<u>na (derived from S2 imagery)</u>
<u>Official fire data</u>	<u>Time log</u>	<u>Report</u>	<u>Depends on fire occurrence</u>	<u>na</u>
<u>Reports of 2017 large wildfires</u>	<u>Guerreiro et al., (2017 and 2018)</u>	<u>Progression polygons</u>	<u>hourly</u>	<u>na</u>

\* depends on aeroplane flight height and on the sensor (visible sensors have higher resolution than IR sensors)

**Table A1A2. Confidence flag value, class and interpretation. The flag is defined for each wildfire.**

<b>Flag value</b>	<b>Flag Class</b>	<b>Interpretation</b>
<b>1</b>	Very Low	The major fire progressions were observed only with satellite data, with important associated uncertainties.
<b>2</b>	Low	The major fire progressions were observed only with satellite data with moderate uncertainties
<b>3</b>	Moderate	The major fire progressions were observed with satellite data with low/moderate uncertainties and complemented with other sources.
<b>4</b>	High	The major fire progressions were at least partially observed with ground and airborne data, with relevant uncertainties associated (e.g. the exact hour of an important progression, or a flank position, etc)
<b>5</b>	Very High	The major fire progressions were observed with ground and airborne data with low uncertainties

**Table A2A3. Database metadata list for L1**

ID	Fire Name	Municipality	Civil Parish	Start Date	End Date	Extent (ha)	Confidence flag	ANEPC incident ID	P1	P2
1	Gouveia_10082015	Gouveia	Mangualde da Serra	2015-08-10	2015-08-12	2513	2	2015090024014	99	86
2	Oleiros_03082015	Oleiros	Alvaro	2015-08-03	2015-08-04	853	2	2015050020535	100	95
3	VilaNovadeCerveira_08082015	Vila Nova de Cerveira	Candemil	2015-08-08	2015-08-09	2988	3	2015160019994	87	87
4	Agueda_08082016	Águeda	Préstimo	2016-08-08	2016-08-12	7317	1	2016010058351	99	63
5	Anadia_10082016	Anadia	V.N. de Monsarros	2016-08-10	2016-08-12	3370	2	2016010059055	97	80
6	ArcosdeValdevez_08082016	Arcos de Valdevez	Cabana Maior	2016-08-08	2016-08-11	5806	1	2016160022311	93	71
7	Arouca_08082016	Arouca	Janarde	2016-08-08	2016-08-14	23547	2	2016010058554	97	96
8	Boticas_05092016	Boticas	Codecoso	2016-09-05	2016-09-07	1694	3	2016170021732/ 2016170021835	97	97
9	CabeceirasdeBasto_06092016	Cabeceiras de Basto	Rio Douro	2016-09-06	2016-09-07	1336	2	2016030067614	100	100
10	Caminha_09082016	Caminha	Argela	2016-08-09	2016-08-11	1628	1	2016160022551	99	61
11	Cinfaes_07082016	Cinfães	Cinfães	2016-08-07	2016-08-08	567	1	2016180042605	95	95
12	Cinfaes_08082016	Cinfães	Oliveira do Douro	2016-08-08	2016-08-09	756	2	2016180042656	100	100
13	FreixodeEspadaaCinta_06092016	Freixo de Espada a Cinta	Freixo Espada à Cinta e Mazouco	2016-09-06	2016-09-07	5194	3	2016040027372	99	97
14	Moncao_06092016	Monção	Riba de Mouro	2016-09-06	2016-09-07	656	2	2016160025950	71	58
15	Moncao_09082016	Monção	Barroças e Taias	2016-08-09	2016-08-11	1115	1	2016160022460	77	77
16	ParedesdeCoura_07082016	Paredes de Coura	Meixedo	2016-08-07	2016-08-12	10457	2	2016160022456	100	96
17	PontedeLima_08082016	Ponte de Lima	Calheiros	2016-08-08	2016-08-09	739	1	2016160022390	91	75
18	SeverdoVouga_09082016	Sever do Vouga	Pessegueiro do Vouga	2016-08-10	2016-08-12	1818	3	2016010058973	96	94
19	VieiradoMinho_10082016	Vieira do Minho	Rossas	2016-08-10	2016-08-11	1637	2	2016030060428	99	96
20	Resende_17082017	Resende	S. Martinho de Mouros	2017-08-17	2017-08-21	544	1	2017180043566	84	38
21	RibeiradePena_15082017	Ribeira de Pena	Cerva	2017-08-15	2017-08-16	507	1	2017170021591	100	100
22	CastroDaire_05102017	Castro Daire	Almofala	2017-10-05	2017-10-05	701	2	2017180054022	99	99
23	Mortagua_07102017	Mortagua	Espinho	2017-10-07	2017-10-08	961	2	2017180054507	99	99
24	Mirandela_16072017	Mirandela	Alvites	2017-07-16	2017-07-17	949	2	2017040020105	100	88
25	Pombal_06102017	Pombal	Abiul	2017-10-06	2017-10-07	1225	2	2017100054724	100	100
26	TorredeMoncorvo_18072017	Torre de Moncorvo	Acoreira	2017-07-18	2017-07-18	1536	3	2017040020365	100	100
27	Guarda_23082017	Guarda	Fernão Joanes	2017-08-23	2017-08-25	3457	3	2017090026098	91	91
28	Serta_08092017	Serta	Pedrogao Pequeno	2017-09-08	2017-09-09	4177	3	2017050027511	100	100

29	Abrantes_09082017	Abrantes	Aldeia do Mato	2017-08-09	2017-08-10	4357	3	2017140045924	83	79
30	CasteloBranco_23072017	Castelo Branco	Santo André das Tojeiras	2017-07-23	2017-07-28	4569	3	2017050023219	97	85
31	Serta_15102017_2	Serta	Pedrógão Pequeno	2017-10-15	2017-10-16	2320	3	2017050030728	54	54
32	CasteloBranco_13082017	Castelo Branco	Lourçal do Campo	2017-08-13	2017-08-15	6173	2	2017050025136	100	96
33	PampilhosadaSerra_06102017	Pampilhosa da Serra	Fajao	2017-10-06	2017-10-09	7217	2	2017060044928	97	96
34	Guarda_17072017	Guarda	Rochoso	2017-07-17	2017-07-18	7523	2	2017090021641	88	88
35	FigueiradaFoz_15102017	Figueira da Foz	Quiaios	2017-10-15	2017-10-17	15141	4	2017060046330	100	97
36	Oleiros_23082017	Oleiros	Cambas	2017-08-23	2017-08-25	7985	3	2017050026111	88	67
37	Gois_17062017	Gois	Alvares	2017-06-17	2017-06-22	15852	3	2017060026571	100	99
38	Alcobaca_15102017	Alcobaca	Pataias	2017-10-15	2017-10-16	18575	4	2017100056537 /2017100056554	100	100
39	Arganil_15102017	Arganil	Coja	2017-10-15	2017-10-16	31970	3	2017060046312 /2017090031521	100	99
40	Serta_15102017	Serta	Figueiredo	2017-10-15	2017-10-17	30974	4	2017050030693	97	97
41	Alvaiazere_11082017	Alvaiazere	Pussos	2017-08-11	2017-08-19	23715	2	2017100043917/ 2017050025201	99	52
42	PedrogaoGrande_17062017	Pedrogao Grande	Pedrogao Grande	2017-06-17	2017-06-19	29456	4	2017100032538	92	91
43	Serta_23072017	Serta	Várzea dos Cavaleiros	2017-07-23	2017-07-27	33401	3	2017050023195	97	96
44	Lousa_15102017	Lousã	Vilarinho	2017-10-15	2017-10-17	45249	4	2017060046260	100	95
45	Agueda_15102017	Agueda	Albitelhe	2017-10-15	2017-10-16	9095	3	2017180056272	83	78
46	OliveiraFrades_15102017	OliveiraFrades	Varzuelas	2017-10-15	2017-10-17	9297	3	2017180056290	99	97
47	Monchique_03082018	Monchique	Monchique	2018-08-03	2018-08-08	26227	3	2018080033743	93	82
48	Agueda_05092019	Agueda	Macinhata do Vouga	2019-09-05	2019-09-06	1602	3	2019010072794	89	84
49	Alijo_24072019	Alijo	Vila Verde	2019-07-24	2019-07-24	574	5	2019170019467	100	100
50	Baiao_04092019	Baião	Teixeira	2019-09-05	2019-09-06	728	3	2019130150620	75	73
51	Nisa_01082019	Nisa	Tolosa	2019-08-01	2019-08-01	712	5	2019120016787	99	98
52	Ourique_10062019	Ourique	Monte Lavarjao	2019-06-10	2019-06-10	554	5	2019020015472	75	75
53	Penedono_21072019	Penedono	Beselga	2019-07-21	2019-07-23	736	4	2019180039496	99	99
54	Sabugal_29082019	Sabugal	Vale Mourisco	2019-08-29	2019-08-29	578	5	2019090029579	100	100
55	Serta_13092019	Sertã	Marmeleiro	2019-09-13	2019-09-14	676	4	2019050028005	100	90
56	Tomar_03082019	Tomar	São Pedro Tomar	2019-08-03	2019-08-03	511	4	2019140045796	86	73
57	Valenca_04092019	Valença	Cerdal	2019-09-04	2019-09-05	642	1	2019160026115	83	83
58	Valpacos_13092019	Valpaços	Ervões	2019-09-13	2019-09-13	738	2	2019170026369	56	56
59	ViladeRei_20072019	Vila de Rei	Fundada	2019-07-20	2019-07-22	9305	3	2019050022178	99	99
60	MirandadoCorvo_13092019	Miranda do Corvo	Moinhos	2019-09-13	2019-09-14	540	3	2019060042282	96	96

61	Fundao_07082020	Fundão	Capinha	2020-08-07	2020-08-08	472	4	2020050018968	87	85
62	Silves_06072020	Silves	Boião	2020-07-06	2020-07-06	520	4	2020080025576	77	77
63	Avis_21072020	Avis	Montes Juntos	2020-07-21	2020-07-21	698	5	2020120014122	95	95
64	IdanhaaNova_30062020	Idanha-a-Nova	Salvaterra do Extremo	2020-06-30	2020-06-30	728	4	2020050015270	100	100
65	SaoJoaoPesqueira_10072020	São João da Pesqueira	Riodades	2020-07-10	2020-07-11	770	4	2020180031783	97	94
66	Fundao_06082020	Fundao	Bogas Baixo	2020-08-06	2020-08-06	749	5	2020050018872	96	96
67	PortoMos_06092020	Porto de Mós	Codacal	2020-09-06	2020-09-07	998	4	2020100046280	97	91
68	OliveiraFrades_07092020	Oliveira de Frades	Antelas	2020-09-07	2020-09-08	1902	3	2020180044235	86	73
69	Aljezur_19062020	Aljezur	Bordeira	2020-06-19	2020-06-20	2243	5	2020080023014	99	93
70	Sernancelhe_06082020	Sernancelhe	Lapa	2020-08-06	2020-08-06	2213	5	2020180037681	100	100
71	Chaves_30072020	Chaves	Vila Verde da Raia	2020-07-30	2020-07-31	2508	3	2020170018342	83	82
72	Oleiros_25072020	Oleiros	Sardeiras de Baixo	2020-07-25	2020-07-27	5564	3	2020050017687	95	92
73	ProencaaNova_13092020	Proenca-a-Nova	Cunqueiros	2020-09-13	2020-09-14	14568	4	2020050022403	91	91
74	CasteloBranco_29082020	Castelo Branco	Ponsul	2020-08-29	2020-08-29	315	4	2020050021105	100	92
75	CastroDaire_07092020	Castro Daire	Cujo	2020-09-07	2020-09-07	452	4	2020180044155	76	76
76	Odemira_18082021	Odemira	João Martins	2021-08-18	2021-08-19	944	5	2021020019189	100	98
77	CastroMarim_16082021	Castro Marim	Pernadeira	2021-08-16	2021-08-17	5956	5	2021080035488	100	99
78	Monchique_17072021	Monchique	Tojeiro	2021-07-17	2021-07-18	1900	4	2021080029244	99	99
79	FreixoEspadaaCinta_20082021	Freixo de Espada à Cinta	Lagoaça	2021-08-20	2021-08-20	412	4	2021040023667	71	71
80	Mogadouro_20072021	Mogadouro	Tó	2021-07-20	2021-07-20	253	5	2021040019425	99	98

p1: stands for percentage of known fire progression (%); p2: stands for percentage fire behaviour descriptors calculated (%)

**Table A3A4. Attribute fields of the fire progressions (L1)**

Field	Description	Possible values
id	Polygon ID	>0
type	Type of Spread Polygon	p - wildfire progression ; z - ignition or active flaming zone ; a - previously burned area
date_hour	Date and hour of the polygon	yyyy-mm-dd hh:mm; uncertain ; na (not applicable)
source	Source of the data	fserv - forest service ; sat - satellite data ; airb - airborne data; fops - fire personnel; ek - expert knowledge; rep - external reports
zp_link	Numerical link between a ignition or active flaming zone (“z”) polygon and a wildfire progression (“p”) polygon	1,2,3... - the link between types "p" and "z" with known dates and hours; 0 - used for type "a" or when progression in "uncertain" or when the link between "p" and "z" is unknown
burn_period	Burning period	1,2,3,..; 0 for the same cases as “zp_link”.

**Table A4A5. Attribute fields of the fire behaviour database -(L2)**

Field	Description	Possible values
fid	Fire ID	1-80*
fname	Fire Name	Municipality_StartDate (e.g. Gouveia_10082015)
year	Year	2015-2021*
type	Type of Spread Polygon	p - wildfire progression ; z - ignition or active flaming zone ; a - previously burned area
sdate	Start date and hour of the polygon	yyyy-mm-dd hh:mm; uncertain ; na (not applicable)
edate	End date and hour of the polygon	yyyy-mm-dd hh:mm; uncertain ; na (not applicable)
inidoy	Start day-of-year of the polygon (hours in decimal values)	1 to 366; -1 for uncertain progression polygons, polygons with unknown zp_link and previously burned areas
endday	End day-of-year of the polygon (hours in decimal values)	1 to 366; -1 for uncertain progression polygons, polygons with unknown zp_link and previously burned areas
source	Source of the data	fserv - forest service ; sat - satellite data ; airb - airborne data; fops - fire personnel; ek - expert knowledge; rep - external reports
zp_link	Numerical link between a ignition or active flaming zone ("z") polygon and a wildfire progression ("p") polygon	1,2,3... - the link between types "p" and "z" with known dates and hours; 0 - used for type "a" or when progression in "uncertain" or when the link between "p" and "z" is unknown
burn_period	Burning period	1,2,3,..; 0 for the same cases as "zp_link".
area	Burned area extent (ha)	> 0 for progression polygons, -1 for ignition or active flaming zones.
growth_rate	Fire growth rate (ha/h)	>0 for progression polygons with zp_link value >0; -1 for previously burned areas or uncertain progression polygons
ros_i	Average rate-of-spread (m/h) calculated since ignition\active flaming areas or a progression marking the start of the burning period	>0 for progression polygons with zp_link value >0; -1 for previously burned areas or uncertain progression polygons
ros_p	Partial rate-of-spread (m/h) calculated between consecutive ignition\active flaming areas and progression polygon, or between two consecutive progression polygons	>0 for progression polygons with zp_link value >0; -1 for previously burned areas or uncertain progression polygons
spdir_i	Spread direction associated with "ros_i" ( ° from North)	0 to 359.99; -1 for the same cases in "ros_i"
spdir_p	Spread direction associated with "ros_p" ( ° from North)	0 to 359.99; -1 for the same cases in "ros_p"

duration_i	Duration (hours) associated with the “ros_i” metric	>0 known progression polygons; -1 for ignition\active flaming zones, previously burned áreas or uncertain progression polygons
duration_p	Duration (hours) associated with the “ros_p” metric	>0 known progression polygons; -1 for ignition\active flaming zones, previously burned áreas or uncertain progression polygons
qc	Confidence flag for each wildfire	See table A1
FRE	Fire Radiative Energy (TJ)	>0 for known progressions with at least 70% of FRE observations between “sdate” and “edate”; - 1 for the remaining polygons
FRE_flux	Fire Radiative Energy flux (TJ ha <sup>-1</sup> h <sup>-1</sup> )	>0 for known progressions with at least 70% of FRE observations between “sdate” and “edate”; - 1 for the remaining polygons
FRE_perc	Percentage of FRE observations between “sdate” and “edate”	Between 0 and 100 for known progression polygons; -1 for the remaining.

\* values will change when the database will be updated with new wildfires.

**Table A5A6. Attribute fields of the simplified fire behaviour database -(L3)**

Field	Description	Possible values
fid	Fire ID	1-80*
fname	Fire Name	Municipality_StartDate (e.g. Gouveia_10082015)
burn_period	Burning period	$\geq 1$
year	Year	2015-2021*
sdate	Start date and hour of the burning period	yyyy-mm-dd hh:mm; "na" for burning periods which only have progression polygons with unknown "zp_link" (see Table A4)
edate	End date and hour of the burning period	yyyy-mm-dd hh:mm; "na" for burning periods which only have progression polygons with unknown "zp_link" (see Table A4)
inidoy	Start day-of-year of the burning period (hours in decimal values)	1 to 366; -1 for burning periods which only have progression polygons with unknown "zp_link" (see Table A4)
endday	End day-of-year of the burning period (hours in decimal values)	1 to 366; -1 for burning periods which only have progression polygons with unknown "zp_link" (see Table A4)
qc	Confidence flag for each wildfire	See table A1
area	Burned area extent (ha)	>0
growth_rate	Average fire growth rate (ha/h)	>0; -1 for burning periods which only have progression polygons with unknown "zp_link" (see Table A4)
ros	Average rate-of-spread (m/h)	>0; -1 for burning periods which only have progression polygons with unknown "zp_link" (see Table A4)
max_ros	Maximum rate-of-spread (m/h) observed in the burning period	>0; -1 for burning periods which only have progression polygons with unknown "zp_link" (see Table A4)
spdir	Spread direction associated with "ros_i" ( ° from North)	0 to 359.99; -1 for burning periods which only have progression polygons with unknown "zp_link" (see Table A4)
duration	Duration (hours) of the burning period	>0; -1 for burning periods which only have progression polygons with unknown "zp_link" (see Table A4)
FRE	Fire Radiative Energy (TJ)	>0 for known progressions with at least 70% of the area burned during the burning period covered with FRE estimates; - 1 for the remaining polygons
FRE_flux	Fire Radiative Energy flux (TJ ha <sup>-1</sup> h <sup>-1</sup> )	>0 for known progressions with at least 70% of the area burned during the burning period covered with FRE estimates; - 1 for the remaining polygons
FRE_perc	Percentage of FRE observations between "sdate" and "edate"	Between 0 and 100

\* values will change when the database will be updated with new wildfires.